universität wien

DIPLOMARBEIT / DIPLOMA THESIS

Titel der Diplomarbeit / Title of the Diploma Thesis

„Characterization of lentivirally transduced human breast cancer cell lines“

verfasst von / submitted by

Erna Jahic

angestrebter akademischer Grad / in partial fulfilment of the requirements for the degree of

Magistra der Pharmazie (Mag.pharm.)

Wien, 2017 / Vienna, 2017

Studienkennzahl lt. Studienblatt / degree programme code as it appears on the student record sheet:	A 449
Studienrichtung lt. Studienblatt / degree programme as it appears on the student record sheet:	Diplomstudium Pharmazie UniStG
Betreut von / Supervisor:	Uni.-Prof. Dipl.-Ing. Dr. Manfred Ogris
Mitbetreut von / Co-Supervisor:	Dr. Haider Sami

For my dearest - my parents Idriz and Kimeta Jahic.

Your names deserve to be written here as much as mine does.

For if it weren't for you and your endless support and encouragement, I wouldn't be standing where I'm standing right now doing the one thing that fulfills me the most

– following my dreams.

Thank you!

♦

♦

Za moje najdraže – moje roditelje, Idriza i Kimetu Jahić.

Vaša imena zaslužuju da budu ispisana ovdje koliko i moje.

Zahvaljujući vama i vašoj beskonačnoj podršci i ohrabrenju, ja sam danas tu gdje jesam i radim ono što me ispunjava najviše

– slijedim svoje snove.

Hvala vam!

♦ ♦ ♦

I would like to take this opportunity to thank all the members of the Macromolecular Cancer Therapeutics Laboratory – I've learned a lot from each and every one of you and I've spent some of the most joyful moments of my pharmacy studies with you! In particular, I would like to express my enormous thanks to Julia Maier for her guidance both in life and science-related matters, and to Dr. Haider Sami for always finding the time to give advice when an advice is most needed. Special thank you to Prof. Manfred Ogris for making it possible for me to learn from him and his research team, and most of all for his kind support at all times.

Table of Contents

1. Introduction

1.1. Breast cancer as a clinically heterogeneous disease

On the list of major death causes in the United States, cancer ranks second after heart disease (Siegel, Miller, and Jemal 2017). According to the predictions made for the year 2017, breast, lung together with bronchus, and colorectal cancer are going to be the 3 most commonly diagnosed cancers for women, collectively contributing to 50% off all new cases of cancer, whereas 30% of it will be attributed to breast cancer only (Siegel, Miller, and Jemal 2017). With 14% estimated deaths in 2017 breast cancer is predicted to be among the leading causes of cancer death in women (Siegel, Miller, and Jemal 2017).

From clinical and molecular points of view, breast cancer is a very heterogeneous disease (Rouzier et al. 2005). The problem with this heterogeneity of breast cancers is that every class shows different sensitivity to pre-operative chemotherapy and also different outcome prognosis (Rouzier et al. 2005). Based on clinical or molecular characterization, breast cancer is usually classified in the following subtypes: hormone-receptor positive (HR+) or luminal, HER2-amplified, and triple negative (TN) or basal-like (Dey et al. 2013). By definition, triple negative breast cancer (TNBC) has negative expression of both estrogen and progesteron receptors, and is negative for HER2 amplification (Dey et al. 2013). However, many studies clearly demonstrate that not all basal-like tumors are TN, and not all TN tumors are basal-like (Gluz et al. 2009). The significant overlap between the two is still present, as there are no standardized clinical markers for clear differentiation (Dey et al. 2013).

According to the estimations, over 170,000 of the 1 million annually estimated breast cancer diagnosis worldwide will be attributed to the triple-negative subtype alone (Anders and Carey 2009). TNBC is associated with a higher grade,

undifferentiated metaplastic histology, stem cell-like characteristics, invasiveness, higher metastatic potential, all which subsequently leads to inconsistency in effectiveness of therapies (Dey et al. 2013) and poor patient prognosis (Gluz et al. 2009).

Cheang et al. (2009) hypothesized that the poor patient prognosis attributed to TNBC may be linked only to the subgroup of basal tumors within the TNBC group. Another important point is the high relapse rate found in clinically treated TNBC patients in the first 3 years after the diagnosis (Ovcaricek et al. 2010). All this and the additional lack of therapeutic options underline the emerging need for immense investigations on TNBC (Dawson, Provenzano, and Caldas 2009).

In this line, as basis for our work we used MDA-MB-231 cell line, which is classified both as TNBC subtype (Pan et al. 2012) and basal-like subtype (Chavez, Garimella, and Lipkowitz 2010), and as counterpart cell line MCF7, which is classified both as hormone-receptor positive (HR+) subtype (Osborne, Hobbs, and Trent 1987) and luminal subtype (Holliday and Speirs 2011).

1.2. The Wnt signaling pathway, and its importance in breast carcinoma

Wnt signaling plays a central role in embryonic development, and is also involved in homeostatic self-renewal in many adult tissues (Clevers 2006). Furthermore, Wnt signaling plays a critical role both in development and in progression of cancers (Koval et al. 2014). Data from Dey et al. (2013) identified Wnt as an active pathway in TNBC.

The Wnt signaling pathway consists of two sub-categories: the canonical Wnt/β-catenin signaling pathway and the non-canonical Wnt signaling pathway (King and Li

2011). Of the two, the canonical Wnt pathway is more critical and studied with greater intensity (MacDonald, Tamai, and He 2009). The functioning of the canonical Wnt/β-catenin signaling pathway revolves around the transcriptional co-activator β-catenin and its levels in the nucleus (MacDonald, Tamai, and He 2009). When Wnt ligands are absent from Wnt receptor, β-catenin degradation complex, consisting of the adenomatous polyposis coli (APC) tumor suppressor, the scaffold protein Axin, the glycogen synthase kinase 3β (GSK3β), and the casein kinase 1 (Ck1) is being assembled (King and Li 2011). This complex leads to phosphorylation, followed by ubiquitination and subsequent degradation of β-catenin by the proteasome (King and Li 2011). However, when Wnt ligands bind to Wnt receptor, the activation of the β-catenin degradation complex and the subsequent β-catenin degradation is inhibited, leading to high cytoplasmic levels of β-catenin (King and Li 2011). This excess of cytoplasmic β-catenin repositions in the nucleus, where it binds to TCF (T cell factor) and promotes the transcription of Wnt target genes upon binding (Clevers 2006). This process is illustrated in detail in the Figure 1, taken from Clevers (2006).

β-catenin mutations or mutations in other Wnt pathway components resulting in β-catenin accumulation, are found in many different human cancers (Howe and Brown 2004). Interestingly, such mutations have not been found very often in breast cancer (Howe and Brown 2004). Nevertheless, Wnt/β-catenin signaling clearly plays a crucial role in breast carcinoma, as this has been supported by many studies (Chung et al. 2004). Moreover, data from Khramtsov et al. (2010) indicate that the deregulation in Wnt/β-catenin signaling is also present in basal-like breast cancers and is an important predictor of decreased overall survival, suggesting that Wnt pathway may be an attractive pharmacological target for this very aggressive subtype of breast cancers.

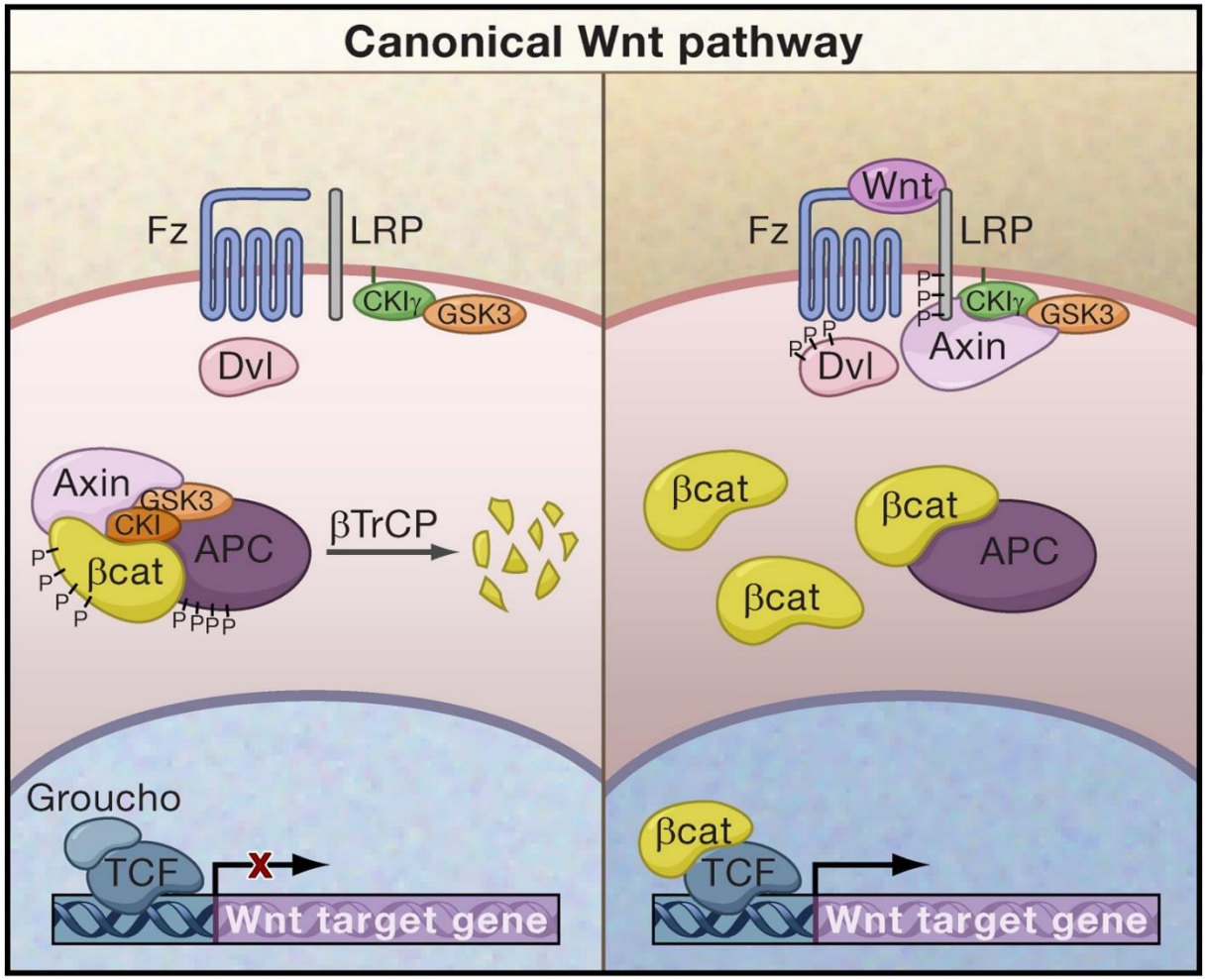

Figure 1. Canonical Wnt/β-catenin signaling, as described in detail by Clevers (2006):

(Left panel) When Wnt receptor complexes are not bound by ligand, the serine/threonine kinases, CK1 and GSK3α/β, phosphorylate β-catenin. Phosphorylated β-catenin is recognized by the F box/WD repeat protein β-TrCP, a component of a dedicated E3 ubiquitin ligase complex. Following ubiquitination, β-catenin is targeted for rapid destruction by the proteasome. In the nucleus, the binding of Groucho to TCF (T cell factor) inhibits the transcription of Wnt target genes. (Right panel) Once bound by Wnt, the Frizzled(Fz)/LRP coreceptor complex activates the canonical signaling pathway. Fz interacts with Dsh, a cytoplasmic protein that functions upstream of β-catenin and the kinase GSK3β. Wnt signaling controls phosphorylation of Dishevelled (Dsh). Wnts are thought to induce the phosphorylation of LRP by GSK3β and casein kinase I-γ (CK1γ), thus regulating the docking of Axin. The recruitment of Axin away from the destruction complex leads to the stabilization of β-catenin. In the nucleus, β-catenin displaces Groucho from Tcf/Lef to promote the transcription of Wnt target genes. (p. 471) Figure from Clevers et al. (2006).

1.3. CTP4 as Wnt pathway-dependent vs. PGK as constitutive promoter

Tumors with constitutive Wnt/β-catenin activation are prospective targets for tumor-specific gene therapy using Wnt pathway-dependent promoters activated by this deregulation (Lipinski et al. 2001). Lipinski et al. (2004) in their study developed the CTP4 promoter consisting of ten Tcf binding sites and a E1B TATA box in the 25bp distance from the proximal one, thus optimizing the activity and specificity profile of the available synthetic β-catenin-dependent promoter. CTP4 showed high β-catenin dependence, with little detectable expression in cells with normal, but high level expression in cells with abnormal β-catenin regulation (Lipinski et al. 2004).

In contrast, constitutive promoters such as mouse phosphoglycerate kinase 1 promoter (PGK) lead to sustained gene expression in both normal and cancer cells, and are widely used for introduction of fluorescent reporter genes such as enhanced green fluorescent protein (eGFP) (Norrman et al. 2010). Moreover, PGK is considered to be a model for high efficiency promoter systems (Graham and Chambers 1997).

Activity of a promoter is strongly dependable on the host cell line type (Qin et al. 2010). The characterization of CTP4 promoter has so far only been conducted with human colon cancer cell lines (Gaedtke et al. 2007), whereas the characterization of PGK promoter has been conducted with various cell lines (Qin et al. 2010), but to our knowledge none of the both were characterized in human breast cancer cell line MDA-MB-231 so far.

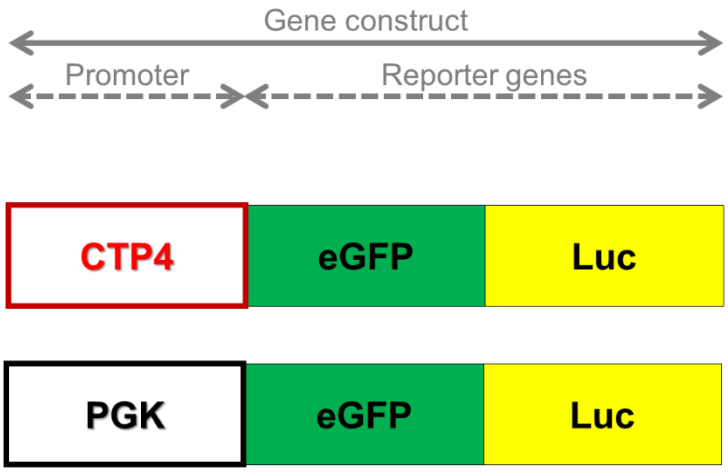

Figure 2. Gene constructs introduced via lentiviral transductions into the human breast cancer cell line MDA-MB-231. This resulted in two human breast cancer cell line subtypes, namely MDA-MB-231 CTP4-eGFPLuc and MDA-MB-231 PGK-eGFPLuc, which we aimed to characterize in this work. CTP4 is a Wnt pathway-dependent promoter (Lipinski et al. 2004), PGK is a constitutive promoter (Qin et al. 2010). eGFP is a widely used reporter gene for the assessment of promoter activity (Norrman et al. 2010) and transgene expression stability (Sumiyoshi et al. 2009). Its fusion to firefly luciferase allows gene expression studies both based on fluorescence (eGFP) or bioluminescence (firefly).

1.4. Lentiviral gene delivery systems

Gene delivery systems are divided into two categories - viral and non-viral gene delivery systems, whereby approximately 70% of the vectors used in gene therapy belong to the viral delivery systems (Chira et al. 2015). Viral delivery vectors originate from different viral classes like adenoviruses (Ad), adeno-associated viruses (AAV), and retroviruses (Chira et al. 2015).

Lentiviruses (LV) are single-stranded RNA viruses derived from human immunodeficiency virus type 1 (HIV-1) (Counsell et al. 2017). As a gene delivery system, they belong to the retroviral vector family, which is traditionally used for stable

overexpression of transgenes or RNA molecules in mammalian cells (Liao et al. 2017), but in contrast to other systems lentiviral vectors are able to transduce both dividing and non-dividing cells (Mátrai, Chuah, and VandenDriessche 2010). Moreover, LV show high transduction efficiency (Hislop et al. 2014) and stable, long-term transgene expression (Kantor et al. 2014), which makes them a prime gene delivery system.

However, integrating gene transfer vectors including lentiviral vectors are known for their semi-random insertion throughout the target cell genome (Berry et al. 2006), subjecting them subsequently to a wide span of genomic environments (Emery 2011). This epigenetic effect of neighbouring genomic sequences and chromatin is termed *chromosomal position effect*, and can often lead to high variegation in expression or gene silencing via histone deacetylation and CpG methylation (Emery et al. 2002). Especially mammalian cells are notorious for exhibiting these transgene repressive effects (Bian and Belmont 2010). Retrovirus variegation with genetically identical sister cells that inherit the same provirus which can either be expressed or silenced, has also been described (Ellis 2005). Moreover, lentiviral vectors are known to integrate variable numbers of proviral DNA copies into cells (Charrier et al. 2011).

In conclusion, our two human breast cancer cell line subtypes obtained via lentiviral transductions are expected to be highly heterogeneous with high variegation in transgene expression patterns, which needs to be characterized in detail.

1.5. Hallmarks of cancer

Six biological capabilities tumor cells acquire during their multistep development are deemed *the hallmarks of cancer*, and they are as follows: sustainment of proliferative signaling, evasion of growth suppressors, resistance to cell death, replicative immortality, induction of angiogenesis, and activation of invasion and metastasis (Hanahan and Weinberg 2000). Recently, two additional emerging

hallmarks have been proposed, namely deregulation of cellular energetics and avoidance of immune destruction (Hanahan and Weinberg 2011).

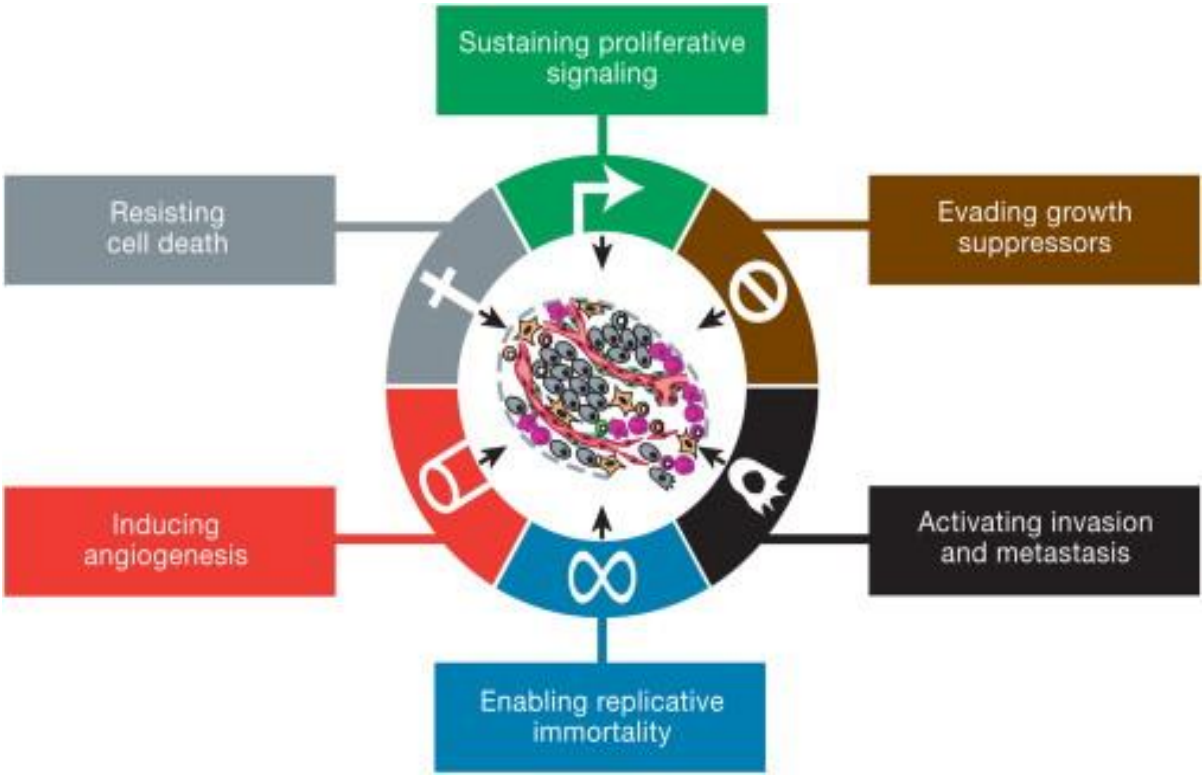

Figure 3. The six hallmarks of cancer originally proposed by Hanahan and Weinberg (2000). In the past decade, two additional emerging hallmarks have been proposed as the next generation of the cancer hallmarks (Figure from Hanahan and Weinberg 2011).

Cancer cells also exhibit the ability to grow under various conditions in cell culture (Mori et al. 2009). Among these, the ability to exhibit anchorage-independent cell growth, or in other words, the ability to form colonies in semi-solid media, has been set in a direct connection with *in vivo* aggressiveness of tumor cells, especially with their tumorigenic potential (Mori et al. 2009). Since transformed cells have the ability to grow anchorage-independent, this type of growth is considered to be yet another hallmark of carcinogenesis by some (Borowicz et al. 2014), and is as such considered to be an *in vitro* cell transformation marker (Mori et al. 2009). The non-adherent colony formation assays are commonly utilized to assess this ability of cells, subsequently allowing the assessment of their tumorigenic potentials *in vitro* (Borowicz et al. 2014).

Tumor metastasis is one of the defining hallmarks of malignant tumors, and a multi-step process during which malignant cells spread far beyond the primary tumor itself by circulating (Talmadge and Fidler 2010). The ability to form metastases is attributed to the migratory ability of malignant cancer cells (Yamaguchi and Condeelis 2007). The *in vitro* scratch assay, with the advantages of simplicity and close reproduction of *in vivo* migration events, is utilized for close observations of this phenomenon (Liang, Park, and Guan 2007).

As the two breast cancer cell line subtypes we aimed to characterize in this work have been genetically altered by lentiviral transgene insertions, it is of great importance to examine their crucial key cancer characteristics in terms of their tumorigenic and metastatic potentials in comparison to the original breast cancer cell line.

2. Aim of the thesis

The overall aim of this work was to characterize the two newly created MDA-MB-231 human breast cancer cell line subtypes, which were gained via lentiviral transductions performed on the original cell line.

A major focus of this work was the assessment of the long-term expression stability of the two lentivirally-inserted transgenes, namely CTP4-eGFPLuc and PGK-eGFPLuc, and the assessment of the activities of the respective promoters for MDA-MB-231 human breast cancer cell line, as to our knowledge this was never done before.

As an additional step, we set up a protocol for single-cell derived cell cultures. We established homogeneous cell line subtypes originating from an isolated single cell of the two original highly heterogeneous cell line subtypes, and subsequently assessed their morphology and transgene expression patterns.

To assess key cancer characteristics of these cell subtypes, we performed anchorage-independent growth assays, namely the soft agar assay, also in comparison to the basal MCF7 cell line. Regarding migratory ability evaluation, we utilized wound healing assays with different serum starvation approaches.

To more closely investigate the growth of individual spheroids, we aimed to set up a protocol enabling us to monitor the growth of a same spheroid in anchorage-independent conditions over time by combinig the standard soft agar colony formation assay with our protocol for single cell culture in a 96 well plate. Lastly, we aimed to test the possibility of utilizing the methyl cellulose assay with MDA-MB-231 cell line and its subtypes.

3. Material and methods

3.1. Reagents

Name	Product number, supplier, location
Agarose, low melting point	A9414, Sigma-Aldrich®, St. Louis, MO, USA
Bovine Serum Albumin (BSA)	A9647, Sigma-Aldrich®, St. Louis, MO, USA
Crystal Violet	C3886, Sigma-Aldrich®, St. Louis, MO, USA
DAPI	D9542, Sigma-Aldrich®, St. Louis, MO, USA
Dulbecco's Modified Eagle's Medium – high glucose	D5671, Sigma-Aldrich®, St. Louis, MO, USA
Dulbecco's Modified Eagle's Medium – low glucose (powder)	D5523, Sigma-Aldrich®, St.Louis, MO, USA
Dulbecco's Phosphate Buffered Saline (PBS)	D8537, Sigma-Aldrich®, St. Louis, MO, USA
Ethylenediaminetetraacetic acid (EDTA)	E6758, Sigma-Aldrich®, St. Louis, MO, USA
Fetal Bovine Serum	F7524, Sigma-Aldrich®, St. Louis, MO, USA Lot No. 064M3396
D(+)-Glucose	346351, Merck Milipore®, Darmstadt, GER
L-Glutamin, 200mM	G7513, Sigma-Aldrich®, St. Louis, MO, USA
Methyl Cellulose	M0512, Sigma-Aldrich®, St. Louis, MO, USA
Paraformaldehyde	A3813.1000, VWR®, Radnor, PA, USA
4-(2-hydroxyethyl)-1-piperazineethanesulfonic acid (HEPES)	A3724.0500, VWR®, Radnor, PA, USA

Sodium bicarbonate	S5761, Sigma-Aldrich®, St. Louis, MO, USA
Sodium chloride	A2942.500, VWR®, Radnor, PA, USA
TrypLE™ Express (1x)	12605010, Gibco®, Grand Island, NY, USA
Versene™ 1:5,000 (1x)	15040033, Gibco®, Grand Island, NY, USA

Table 1. List of reagents.

3.2. Cell culture

All of the cell lines used for the experiments originate from a Caucasian human mammary gland and were isolated from a malignant pleural effusion as the metastatic site of adenocarcinomas. MCF7 cell line (Product No. 86012803; ECACC®, Salisbury, UK; original passage from manufacturer: 18) is classified as a luminal epithelial and MDA-MB-231 cell line (Product No. 710405391; ATCC®, Manassas, VA, USA, original passage from manufacturer: 38) as a basal-like epithelial cell type.

The two of the MDA-MB-231 cell line subtypes used for the experiments, namely MDA-MB-231 CTP4-eGFPLuc and MDA-MB-231 PGK-eGFPLuc, were obtained by performing lentiviral transductions on MDA-MB-231 cells. This was done by Julia Maier (University of Vienna, Austria) and PD Dr. Martina Anton (Technical University of Munich, Germany). Subsequent cell sorting was performed by Julia Maier and Dr. Christian Winter (University of Vienna, Austria) using FACS Ariall (BD Biosciences, San Jose, CA, USA).

Passage numbers of the cell lines used for the experiments were as following: MCF7 34-68, MDA-MB-231 wild type 58-93, MDA-MB-231 CTP4-eGFPLuc 54-88, MDA-MB-231 PGK-eGFPLuc 54-87.

All cell lines were cultured in 25/75/150cm² tissue culture treated flasks (83.3910.002/11.002/12.002, Sarstedt, Nümbrecht, GER), depending on number of cells needed at given timepoint. The culture medium consisted of DMEM high glucose 10% FBS 0.584 g/L L-glutamine. Cells were kept in a humidified incubator at 37°C and 5% CO_2. Upon 90% confluency, old medium was discarded, dead cells were washed off by careful pipetting of 1/2/3ml PBS into one corner of flask, followed by gentle distribution over the surface of flask containing attached cells. Cells were detached by 4 minutes long incubation in humidified incubator at 37°C and 5% CO_2 with 0.5/1/1.5ml of appropriate detaching reagent, followed by gentle tapping and visual control under microscope. Detaching reagent was either TrypLE™ Express for MCF7, or Versene™ for MDA-MB-231 and its subtypes. Detached cells were collected using 2.5/5/7.5ml culture medium and transferred into centrifuge tube for centrifugation at 200 times the gravitational force (x *g*) for 5 minutes at room temperature. Supernatant was discarded, and the pellet resuspended in 1,000µl 37°C culture medium or, if required, in 1,000µl 37°C lab-made PEB solution, which is the mixture of PBS, 2mM EDTA solution and 0,5% BSA. This solution is used to minimize the clumping of the cells to one another, and the attachment to the walls of tubes. The desired fraction (mostly 1/4, 1/5 or 1/6 of the total cell suspension) was then seeded into a new cell culture flask containing already conditioned culture medium, and incubated.

3.3. Expression stability of the lentiviral transgenes

The following measurement was usually performed weekly. Upon 90% confluency, the cells of MDA-MB-231 wild type, MDA-MB-231 CTP4-eGFPLuc and MDA-MB-231 PGK-eGFPLuc were detached with Versene™ according to chapter 3.2. After the centrifugation step, pellets were resuspended in 1ml 37°C PEB solution.1/10 of each cell suspension was transferred into separate round bottom polystyrene test tubes (352008, Corning®, Corning, NY, USA) containing 900µl of ice-cold PEB

solution. These samples were then either kept at 4°C prior to measurement or directly measured via flow cytometry (MACSQuant® Analyzer 10, MACS Miltenyi Biotec, Bergisch Gladbach, GER) with the following settings: FSC lin 235V, SSC lin 310V, B1 hlog 280V, B3 hlog 340V. The machine was set to thoroughly mix the samples and to take up 100µl in order to measure approximately 10,000 cells.

Every third week the fraction remaining after seeding for onward culturing and sample-preparation for flow cytometry measurement of all three cell types used here was frozen at -150°C as a back-up plan.

From day 56 on, DAPI was used as live-dead stain. Samples were then prepared by transferring 1/10 of each cell suspension into a separate reaction tube containing 300µl of ice-cold PEB solution, and adding 100µl of 5µg/ml DAPI solution immediately prior to the measurement. The measurement settings remained the same with the exception of the additional measurement in V1 at hlog 466V.

The analysis of the flow cytometry data was performed using FlowJo® X (version 10.0.7, 32bit, www.flowjo.com). For an example of the gating strategies both with and without DAPI stain see Figures 4. and 5. In the first gate (FSC-A, SSC-A) cell debris was gated out, and in the second gate (FSC-A, FSC-H) doublets were gated out. In the experiments where DAPI was used, dead cells were then gated out in the third plot (V1-A, FSC-A). From this, the fraction of eGFP- cells and also the fraction of cells giving the signals in B1 and B3 channels only due to their autofluorescence were gated out in the fourth gate (B1-A, B3-A) and the percentage of eGFP+ cells was determined by comparison to the MDA-MB-231 wild type sample. The fraction of eGFP- cells was also gated out using a histogram (B1-A, count) as a mean for data display. The identical gating strategy was applied throughout the entire experiment. Also, the median eGFP-signal intensity (in relative units) among the eGFP+ cell population was calculated by the program.

The results were then visualized with GraphPad Prism 6 (version 6.01, www.graphpad.com).

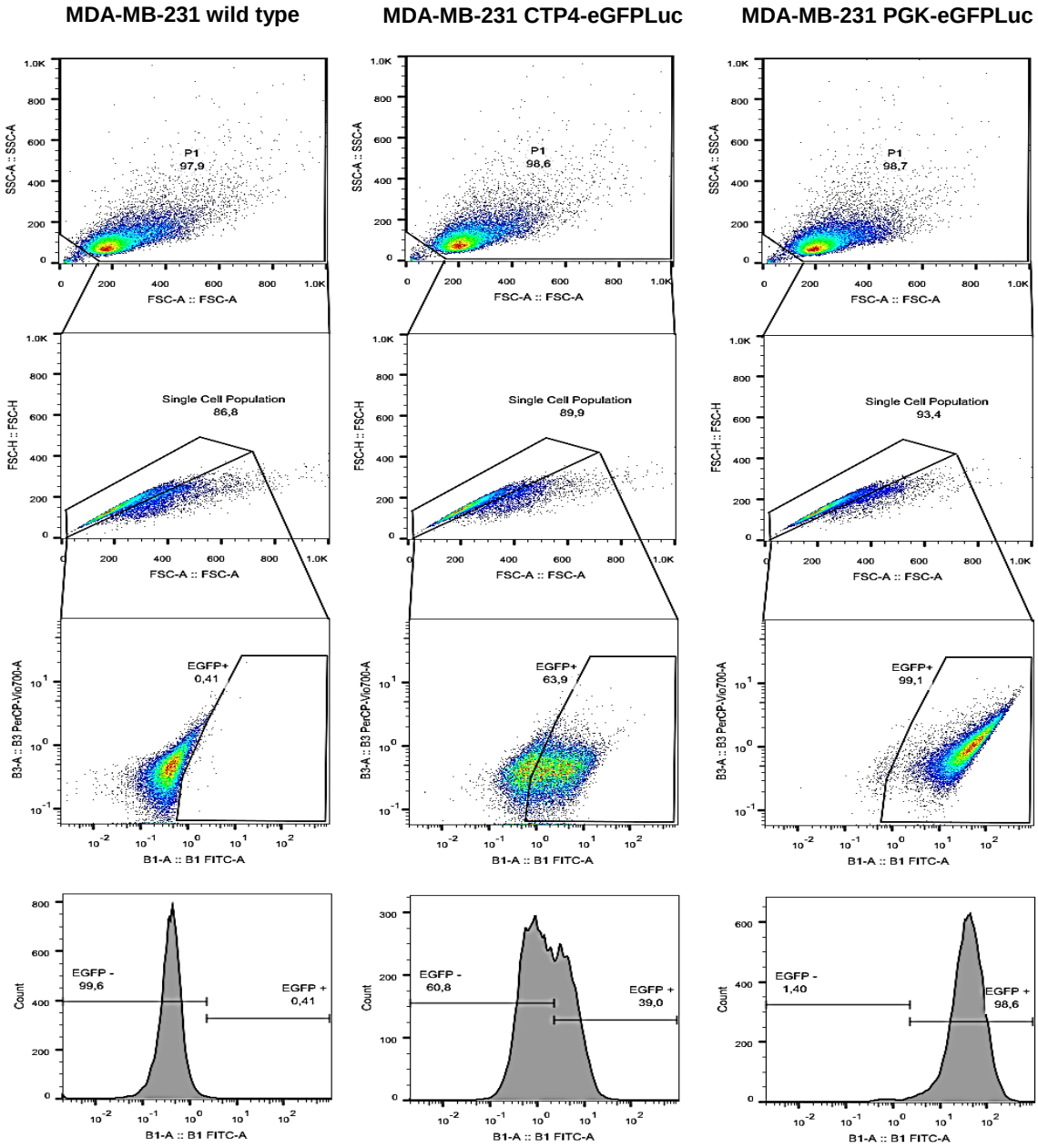

Figure 4. Gating strategy for lentiviral transgene stability analysis, without DAPI. The left column shows the analysis of MDA-MB-231 wild type cell line, the middle column the analysis of MDA-MB-231 CTP4-eGFPLuc cell line subtype, and the right column the analysis of MDA-MB-231 PGK-eGFPLuc cell line subtype. With the first gate named P1 (first row) and the second gate named Single Cell Population (second row), cell debris and doublets were removed. By gating out eGFP- cells (both third and fourth row) in MDA-MB-231 wild type cell line and applying the same gate on MDA-MB-231 CTP4-eGFPLuc and MDA-MB-231 PGK-eGFPLuc subtypes, the percentage of eGFP+ cells in the cell line subtypes was determined. Also, among this cell debris-free, doublets-free and eGFP+ population, the mean eGFP signal intensity was calculated by the program. This gating strategy remained the same throughout the entire part of the experiment without DAPI as live-dead stain.

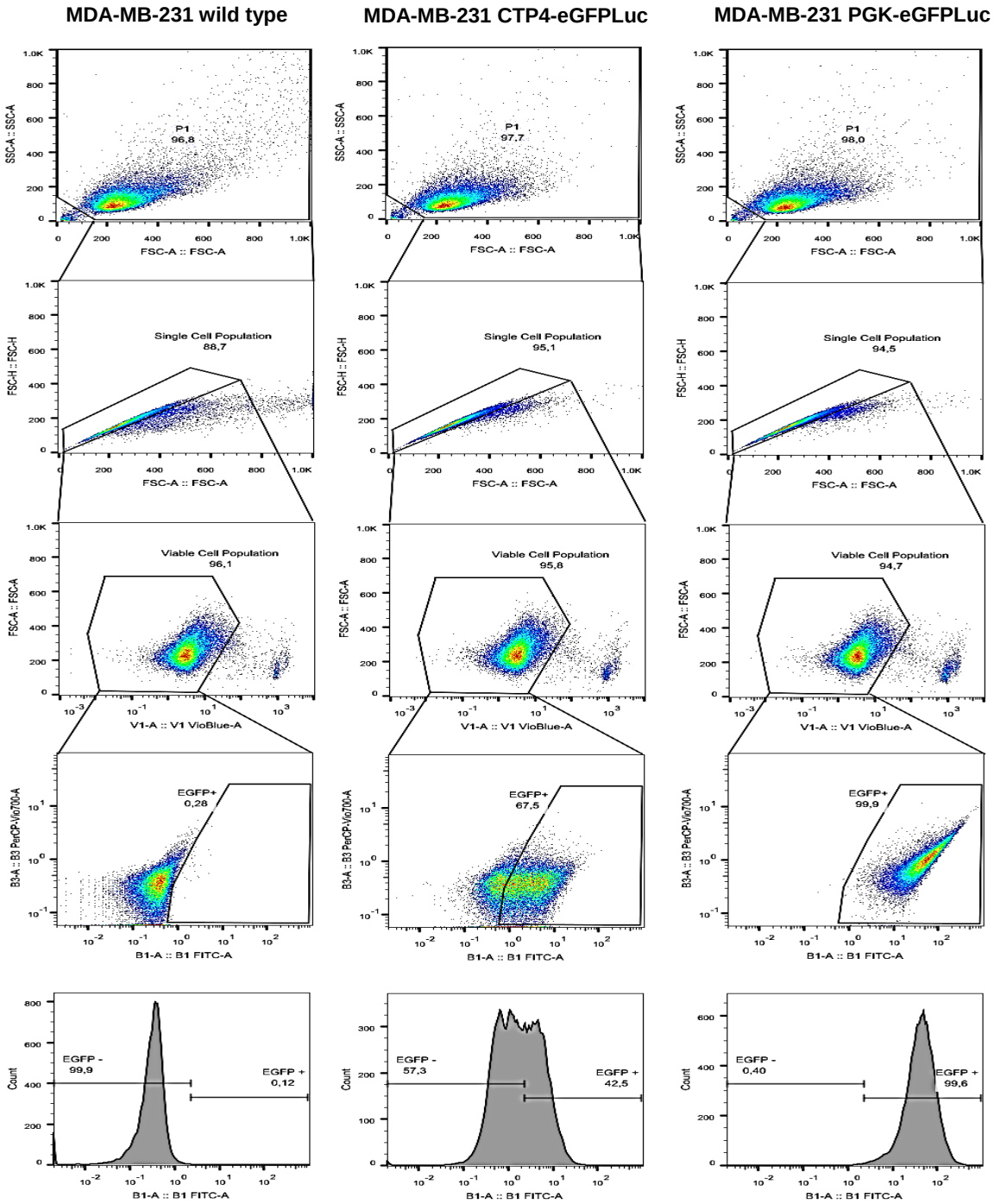

Figure 5. Gating strategy for lentiviral transgene stability analysis, without DAPI. The left column shows the analysis of MDA-MB-231 wild type cell line, the middle column the analysis of MDA-MB-231 CTP4-eGFPLuc cell line subtype, and the right column the analysis of MDA-MB-231 PGK-eGFPLuc cell line subtype. The gating strategy remained the same to the one described in Figure 4. with the exception that among the single cell population (second row), dead cells stained with DAPI were excluded (third row), and then the percentage of eGFP+ cells and the median eGFP-signal intensity in both of the cell line subtypes were determined as described in Figure 4. This gating strategy remained the same throughout the entire part of the experiment with DAPI as live-dead stain.

3.4. Single cell culture (SCC)

For the purposes of this experiment frozen stocks of both MDA-MB-231 CTP4-eGFPLuc and MDA-MB-231 PGK-eGFPLuc with the lowest passage numbers (p57 and p55 respectively) were thawed up and seeded in culture flasks for a recovery in a humidified incubator at 37°C and 5% CO_2. Upon 90% confluency, cells were detached according to the method described in the chapter 3.2. Cells were then counted in a Neubauer chamber (0640010, Marienfeld-Superior, Lauda-Königshofen, GER). Cells were seeded in a manner consistent with every third well containing one cell. To ensure the correct pipetting of the exact cell number needed for seeding, we followed a serial dilution rationale. A first fraction of the cell suspension containing either 36,000 or 72,000 cells was transferred into a 1.5ml microcentrifuge tube and filled up to 1,000µl with culture medium (Table 2, “Cell Suspension (1)” and “Cell Suspension (2)” respectively). Then, the respective dilution series from Table 2. were performed.

Step	Amount Transferred	Source	Diluent (Culture medium) Amount	Dilution Step	End Cell Number
1	10µl	Cell Suspension (1)	990µl	1:100	360
2	100µl	#1	900µl	1:10	36

or

Step	Amount Transferred	Source	Diluent (Culture medium) Amount	Dilution Step	End Cell Number
1	10µl	Cell Suspension (2)	990µl	1:100	720
2	100µl	#1	900µl	1:10	72
3	500µl	#2	500µl	1:2	36

Table 2. The respective dilution series for single cell culture.

The 1,000µl of cell suspension containing 36 cells were then transferred to a sterile plastic reservoir pre-filled with 23ml of warm culture medium. Cell suspension was mixed thoroughly but gently by pipetting up and down for several times with a 25ml serological pipet and then each well of a 96 well plate (655160, Greiner bio-one™, Frickenhausen, GER) was evenly filled with 200µl of this cell suspension with a multichannel pipet by using the reverse pipetting technique. Between each pipetting step, the cell suspension was mixed up thoroughly with the multichannel pipet to ensure an even distribution of cells. The plate was then incubated at 37°C and 5% CO_2.

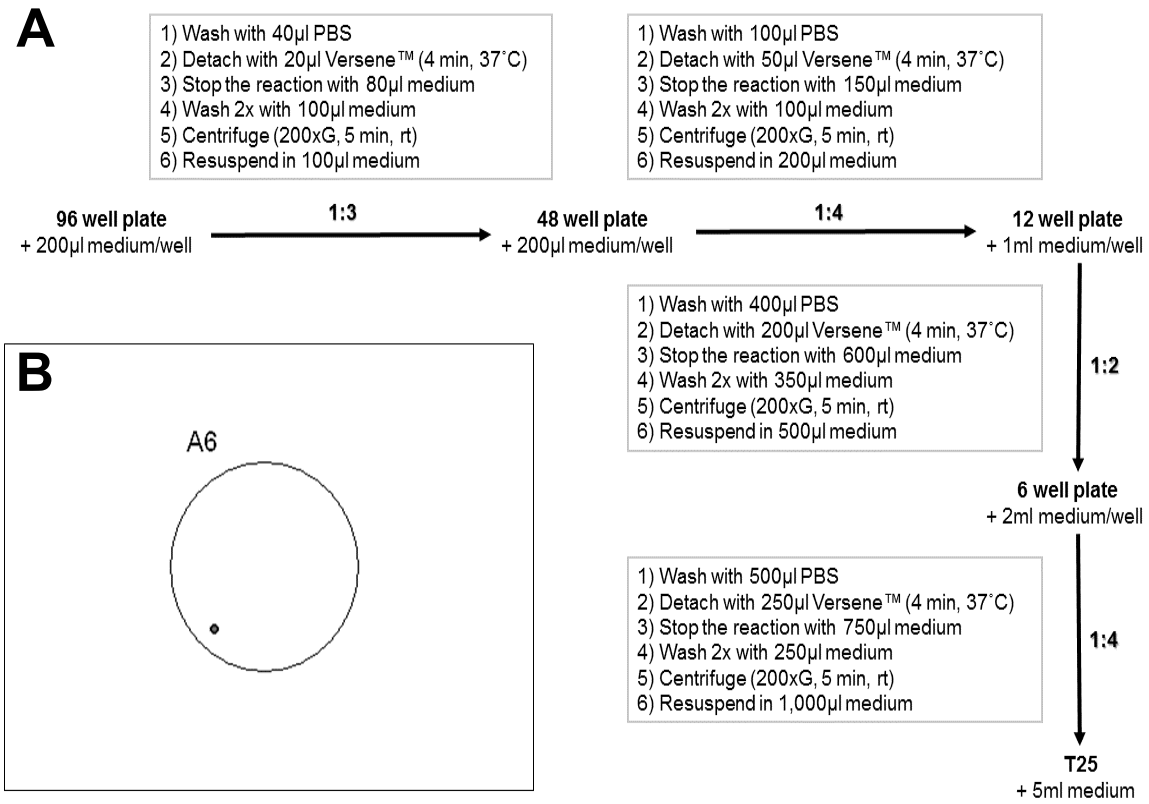

Figure 6. Culturing approach for single cell culture. A) The scheme of successive transfers made to 48, 12, 6 well plates and T25 tissue culture flask while establishing a culture originating from a single cell, indicating the exact amounts of PBS, Versene™ and medium used for each transfer respectively. B) An example of the schematic illustration indicating a position of a single cell in a well together with well name used for easier observation of wells.

On the next morning, wells were observed in detail under light microscope (Motic® AE31 series Microscope) with 10x objective and pictures were taken with Moticam 3.0MP camera (Motic Electric, Xiamen, China). For the wells containing single cells, a schematic illustration was drawn indicating a position of a single cell in a well together with the well name (Figure 6B). In the following days, these illustrations were used to closely observe the wells in question to see if single cells have started to form cultures of their own.

75% of culture medium volume were exchanged every 3rd day, and at the same time cells were gently detached by pipetting to facilitate an even cell spread over the well bottom, preventing clustering and subsequent cell death.

Upon 90% confluency, cells were transferred to a 48 well plate (677180, Greiner bio-one™, Frickenhausen, GER) following the steps described in the chapter 3.2, but the amounts of PBS, Versene™ and culture medium used here were adapted to the well format. The same was done for the successive transfers made to a 12 well plate (665180, Greiner bio-one™, Frickenhausen, GER), 6 well plate (657160, Greiner bio-one™, Frickenhausen, GER) and 25cm² tissue culture treated flask. For the exact amounts used for each transfer see Figure 6A.

Later on, samples were prepared and measured using MACSQuant® Analyzer 10 with the same settings, as described in the chapter 3.3. The analysis of the data was performed with FlowJo® X by applying the same gating strategy used for the measurements in which DAPI was used as live-dead stain, as described in the chapter 3.3. (Figure 5) and the results were then visualized with GraphPad Prism 6.

3.5. Non-adherent colony formation assays

3.5.1. Soft agar colony formation assay

For the soft agar colony formation assay a modified protocol of Borowicz et al. (2014) was used. The assay was performed in non-adherent 6 well plates (CC7672-7506, USA Scientific, Ocala, FL, USA) and two times in total. Once 5,000 cells per well, and once 2,142 cells per well, each in triplicates for each cell line, were seeded. For this experiment we used MCF7, MDA-MB-231, and the two MDA-MB-231 subtypes mentioned in chapter 3.2.

Plastic-covering and attachment-preventing bottom layer was set to 0.5% and cell-containing top layer to 0.3% low melting point agarose by liquefying 3% low melting point agarose stocks in heating block at 70°C and 300 rounds per minute for 10 minutes and diluting it in a fast manner with pre-heated (37°C) mixture of 2x culture medium 20% FBS and ddH_2O. The exact ratios for this were set to (1) achieve respective soft agar concentrations, and at the same time to (2) reach normal 1x medium 10% FBS culture conditions in the end concentration. After pouring the bottom layer (1ml per well), plates were kept at 4°C at least for one overnight before proceeding with top layer pouring (2ml per well) with concurrent seeding of cells previously added to this top layer mixture. Afterwards, plates were first kept at room temperature for 30 minutes, then incubated at 37°C and 5% CO_2 for 21 days. In those 21 days, cells were fed with 100µl culture medium per well 2 times a week.

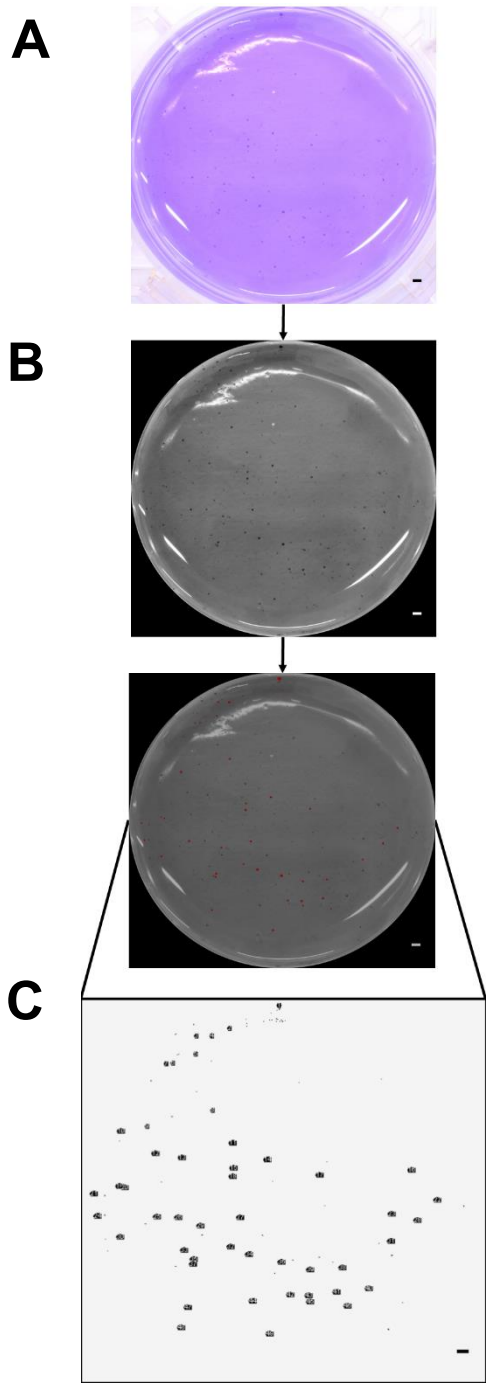

Figure 7. Evaluation of soft agar colony formation assay in ImageJ®. A) Cells were fixed with formaldehyde, stained with crystal violet, and each well was imaged separately (Canon EOS 6D with Canon Macro Lens EF 100mm). B) Pictures were processed in ImageJ® for the purpose of simplified and reproducible counting in an automated fashion: firstly pictures were converted to 16-bit format, secondly only the well surface was marked by the Oval tool, and outside was cleared with the Clear Outside command. Then, the threshold was set between 50 and 178 (using the Image -> Adjust -> Threshold command sequence) to mark spheroids intended for counting. C) Only marked spheroids in red with diameters in the range of 100µm to 500µm were counted automatically by using Analyze -> Analyze Particles and setting the size to surface areas of circles with respective diameters in µm², and surface area for each of those was measured individually.
ImageJ® was priorly calibrated using a picture of a millimeter paper taken together with well pictures.
Scale bar is set to 1,000µm.

At the 21-day endpoint, created spheroids were fixed with 1ml 4% (w/v) formaldehyde in HBS for 15 minutes at room temperature. The 4% (w/v) formaldehyde fixation solution was prepared as follows: paraformaldehyde was dissolved under magnetic stirring in HBS (20mM HEPES, 150mM sodium chloride, pH 7.1), pH value was adjusted to 7.0-7.5, then the mixture was filtered through pleated filter and stored at 4°C. After the PFA fixation step, samples were stained by using 1.5ml 0.005% crystal

violet in PBS, for 15 minutes at room temperature. The wells were then washed with 2ml PBS twice. Spheroids were imaged with Motic AE31 series microscope with Moticam 3.0MP, and 4x and 10x objectives to determine the representative sizes, and with a camera (Canon EOS 6D with Canon Macro Lens EF 100mm) to count the total number of created spheroids per well and their size distribution. Both sets of pictures were evaluated in ImageJ® (V 1.49, 32-bit, www.imagej.nih.gov/ij) (Figure 7).

3.5.2. Soft agar colony formation assay in combination with single cell culture

Even though the soft agar colony formation assay in usual 6 well plate format is a very useful tool to observe differences among cell types regarding number of created unicellular-originated colonies at the endpoint and their size distribution, it does not offer the possibility to follow the growth of an individual unicellular-originated spheroid over time. To overcome this limitation the soft agar colony formation assay in combination with single cell culture was successfully attempted.

For this try-out experiment a modified protocol of Borowicz et al. (2014) optimized to fit a 96 well plate format was used, and combined with the protocol for single cell culture described in detail in the chapter 3.4. The assay was performed in 96 well plates (655160, Greiner bio-one™, Frickenhausen, GER) and with MDA-MB-231 PGK-eGFPLuc subtype.

For preparation of bottom layer 1% low melting point agarose was used, diluted to 0.5% with 2x culture medium, and 30µl per well were pipetted using the reverse pipetting technique, as a minimum for complete covering of the well bottom. For preparation of the top layer, 0.6% low melting point agarose was used, diluted to 0.3%

with 2x culture medium containing the intended cell number, and 120µl per well were pipetted using the reverse pipetting technique. In this way, an optimal total layer height including bottom plastic of 7mm was achieved, as this was a necessary requirement for effective microscopy imaging.

Regarding the seeded cells, a dilution series was again performed. Starting with 300,000 cells and diluting this number to 300 cells in final 100µl of 2x culture medium, cells were seeded in a manner consistent with every well containing two cells.

The next morning, wells were observed in detail. For wells containing cells, a schematic illustration was drawn, indicating the approximate position of cells in wells together with the well name (Figure 6B). In the following days, these illustrations were used to closely monitor the development of spheroids. Pictures were taken with Motic AE31 series microscope with Moticam 3.0MP and EVOS® FL Imaging System (AMF4300, ThermoFisher Scientific, Waltham, USA), and evaluated in ImageJ®.

Once a week cells were fed by adding 5µl of pre-warmed culture medium.

3.5.3. Methyl cellulose assay

For the methyl cellulose assay, the protocol that was a kind gift of Angelika Walzl (Medical University of Vienna, Austria) was used. On day one, methyl cellulose-containing medium was prepared by dissolving 15g of autoclaved methyl cellulose in 500ml pre-heated DMEM high glucose no additives with the help of stirring (20 minutes at 750 speed and room temperature). Then, additional 500ml of DMEM high glucose and the appropriate amount of L-glutamine for 1l DMEM were added under sterile conditions, and stirred (overnight at 250 speed and 4°C). On the next day, aliquots of this mixture were centrifuged for 2 hours at 4,700 times gravitational force (x *g*) at room

temperature. Afterwards, clear and viscous supernatant was separated, and stored as aliquots at -20°C.

For spheroid generation, cells of MCF7, MDA-MB-231 wild type and its two subtypes were detached according to the chapter 3.2. and counted in a Neubauer chamber. For each cell line, the amount of cell suspension needed for 100 wells à 3,000 cells was calculated, and added to centrifuge tube pre-filled with 2ml of methyl cellulose-containing medium. Then, culture medium 10% FBS was added to 10ml total volume, and gently mixed, without additional FBS adjustment for the 2ml of methyl cellulose-containing medium. 100µl/well of this mixture were then pipetted to a non-treated U-bottom 96 well plate (650101, Greiner bio-one™, Frickenhausen, GER). Well plates were then centrifuged for 10-20 minutes at 1,000-1,500x *g* at room temperature, and put in the humidified incubator at 37°C and 5% CO_2 for 24 hours.

24 hours after generation, multicellular spheroids were harvested by transferring the entire medium of each well into a reservoir with a multichannel pipet, with 200µl tips. This medium contained the spheroids. It was then transferred into a 50ml tube, and centrifuged for 3 minutes at 100x *g*, at room temperature. Supernatant was aspirated, and the spheroid pellet was resuspended in 1ml culture medium.

Both before and after harvesting, created multicellular spheroids were observed under light microscope (Motic® AE31 series Microscope) with a 10x and 20x objective, and pictures were taken with a Moticam 3.0MP camera.

3.6. Scratch assay

In tissue culture treated 6 well plates (657160, Greiner bio-one™, Frickenhausen, GER), 500,000 cells of MDA-MB-231, or the two subtypes MDA-MB-

231 CTP4-eGFPLuc and MDA-MB-231 PGK-eGFPLuc, were seeded in triplicates in 1ml culture medium per well. They were then incubated at standard conditions. This was done in two experiments with two different starvation approaches for cell cycle synchronization (Pirkmajer and Chibalin 2011; Pontarin et al. 2011), since we also wanted to test which setting works better for this cell line.

In the first experiment, cell starvation was performed with 1ml culture medium with only 2% FBS per well, and cells were incubated starting in the night prior to scratch infliction. Cells were kept under these conditions for the imaging. In the second experiment, cell starvation was performed with 1ml culture medium without FBS per well, and cells were incubated for 24 hours starting on the first morning after the seeding day. For imaging, cells were kept in 1ml culture medium containing 10% FBS.

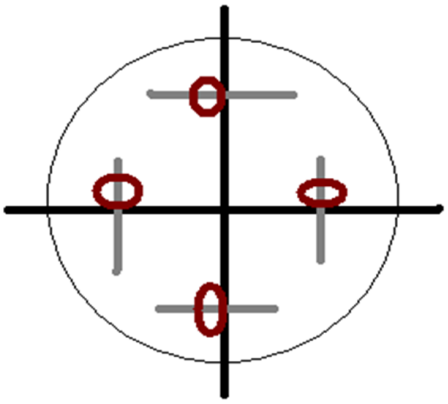

Figure 8. Scratch assay method. The cross in black was made with an ethanol-resistant marker prior to seeding on the bottom of the well plate. Positions in grey indicate where scratches were generally inflicted. Usually, 3-4 scratches were inflicted on each side of the cross. Positions in red indicate targeted areas for pictures.

Upon 90% confluency, several straight scratches were inflicted with a 10µl pipette tip under sterile conditions, in a manner illustrated representatively in Figure 8. Scratched cells were removed by careful washing of wells with 1ml PBS for two times. Scratches were imaged at timepoints 0h, 6h, 24h, 30h, 48h after scratch infliction and with EVOS® FL Imaging System in the first experiment, and at timepoints 0h, 5h, 24h, 30h, 48h after scratch infliction with Motic AE31 series microscope with Moticam 3.0MP in the second experiment, and with 4x objective in both.

TScratch software (Gebäck et al. 2009) was used for data evaluation, then the results were visualized with GraphPad Prism.

4. Results

4.1. Lentivirally transduced inserts of PGK-eGFPLuc were not affected by gene silencing over a four-month time period

To examine whether or not the gene silencing of the two lentivirally introduced gene constructs, namely CTP4-eGFPLuc and PGK-eGFPLuc, in MDA-MB-231 cells occurs, the percentage of the cells expressing eGFP and the intensity of the eGFP signal per eGFP-expressive cell were analyzed weekly over a four-month time period by flow cytometry. In addition to this, the activities of the respective promoters in this cell line were assessed.

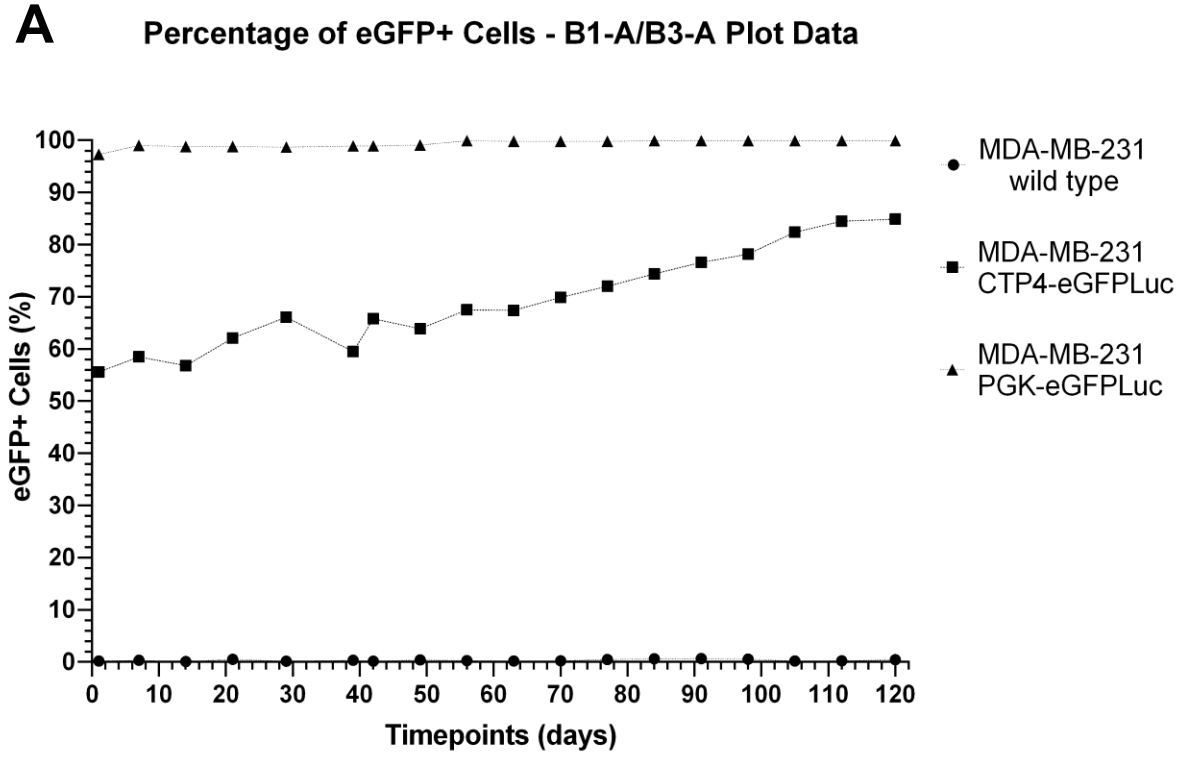

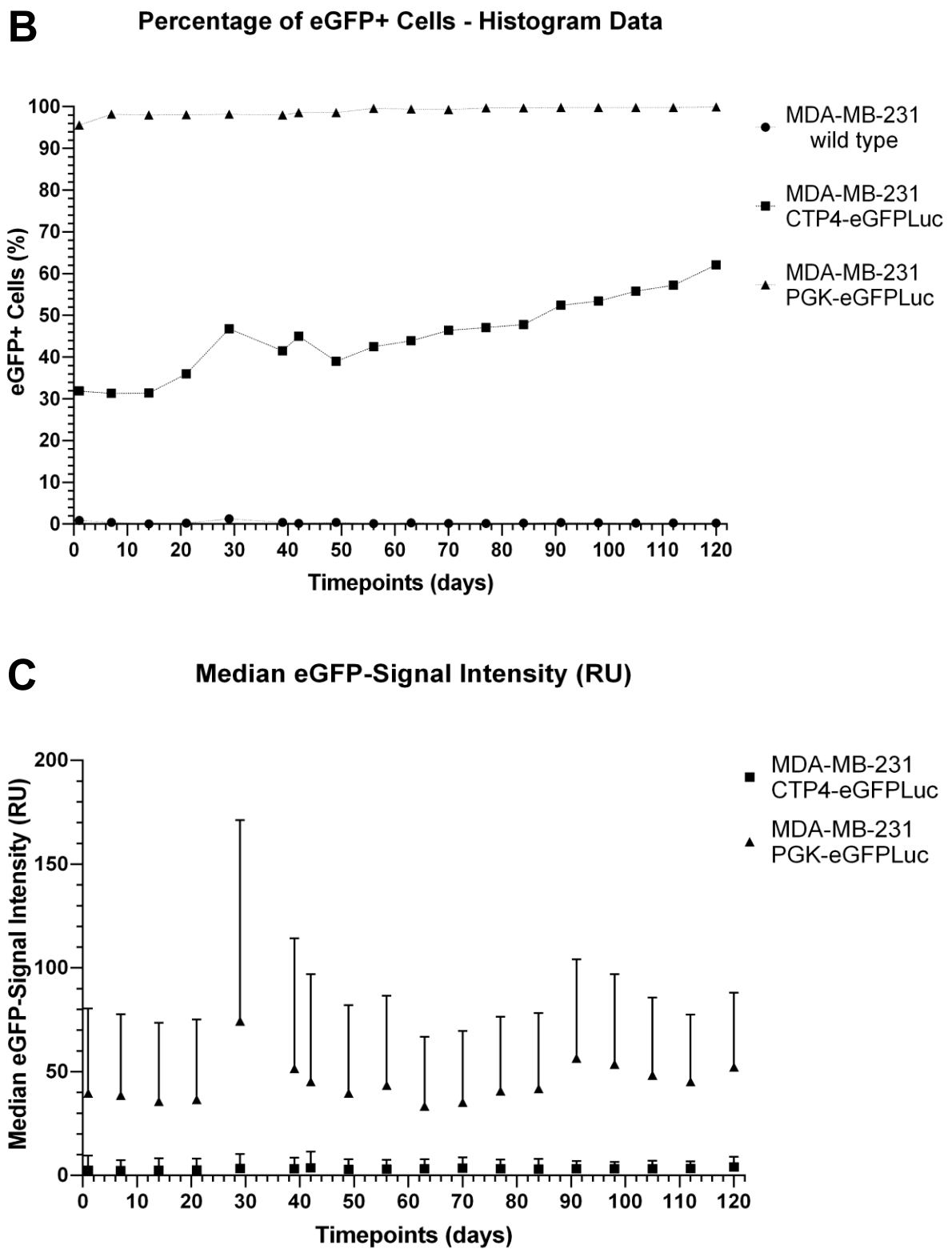

Figure 9. Flow cytometry measurements for MDA-MB-231 wild type, MDA-MB-231 CTP4-eGFPLuc, and MDA-MB-231 PGK-eGFPLuc over a four-month time period. A) The percentage of eGFP+ cells based on B1-A/B3-A-plot data. B) The percentage of eGFP+ cells based on B1-A-histrogram data. C) The median eGFP-signal intensity per eGFP+ cell calculated by FlowJo®. Error

bars represent the standard deviation from approximately 10,000 measured cells. A) and B) Data represent one measurement per condition on respective days.

The results of the 4-month-measurements from both B1-A/B3-A-plot and B1-A-histogram data showed that the percentage of eGFP+ cells in MDA-MB-231 PGK-eGFPLuc remained constant in its value near 100% over this time period (Figures 9A and B). In accordance to this, the median eGFP-signal intensity showed no dramatic changes over this time period (Figure 9C). These two results combined led to conclusion that no gene silencing of the PGK-eGFPLuc transduct in MDA-MB-231 cell line has occurred in the time period of 4 months.

At the very beginning of the experiment, the percentage of eGFP+ cells in MDA-MB-231 CTP4-eGFPLuc was at around 55% according to the B1-A/B3-A-plot data, or at around 32% according to the B1-A-histogram data (Figures 9A and B). Both plots showed the significant increase in the percentage of eGFP+ cells, leading to respectively 85/62% of the eGFP+ cells at the end of the experiment (Figures 9A and B). The median eGFP-signal intensity showed however no clear changes over this period of time (Figure 9C). We speculate that the increase in eGFP+ cells in MDA-MB-231 CTP4-eGFPLuc could have happened either due to increased proliferation of the eGFP+ cells, or due to activation of the Wnt signaling pathway in the originally non-eGFP+ cells. In contrast to the PGK-eGFPLuc data presented above, we cannot offer definite conclusions on the gene silencing status of CTP4-eGFPLuc inserts, as the remaining cell population positive for this insert but due to the inactivity of their Wnt pathway not also eGFP+ cannot be measured.

The comparison of the measured strengths of the median eGFP-signal intensities per eGFP+ cell in the two cell line subtypes shows the PGK is the stronger promoter of the two, with the values in the range between 40 and 60 relative units, whereas the CTP4 manifests values in the range between only 2 and 4 relative units (Figure 9C).

However, the standard deviation for all the measurements in both cell line subtypes is extremely high (Figure 9C). This strongly variable individual signal strength correlates with the expected heterogeneity of cells transduced via lentiviruses.

A

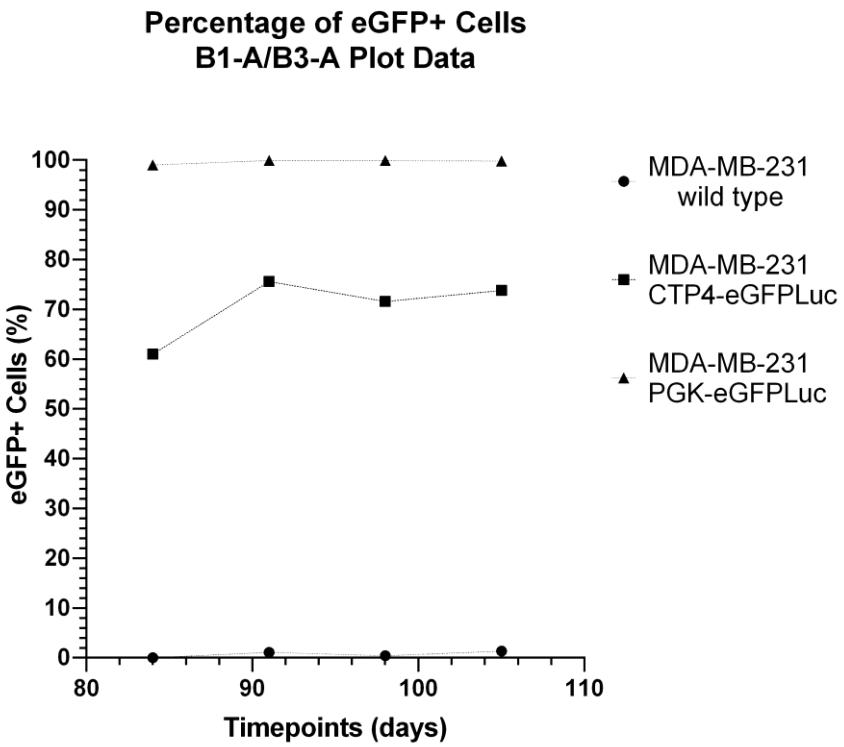
Percentage of eGFP+ Cells
B1-A/B3-A Plot Data
eGFP+ Cells (%)
100
90
80
70
60
50
40
30
20
10
0
80
90
100
110
Timepoints (days)
MDA-MB-231
wild type
MDA-MB-231
CTP4-eGFPLuc
MDA-MB-231
PGK-eGFPLuc

B

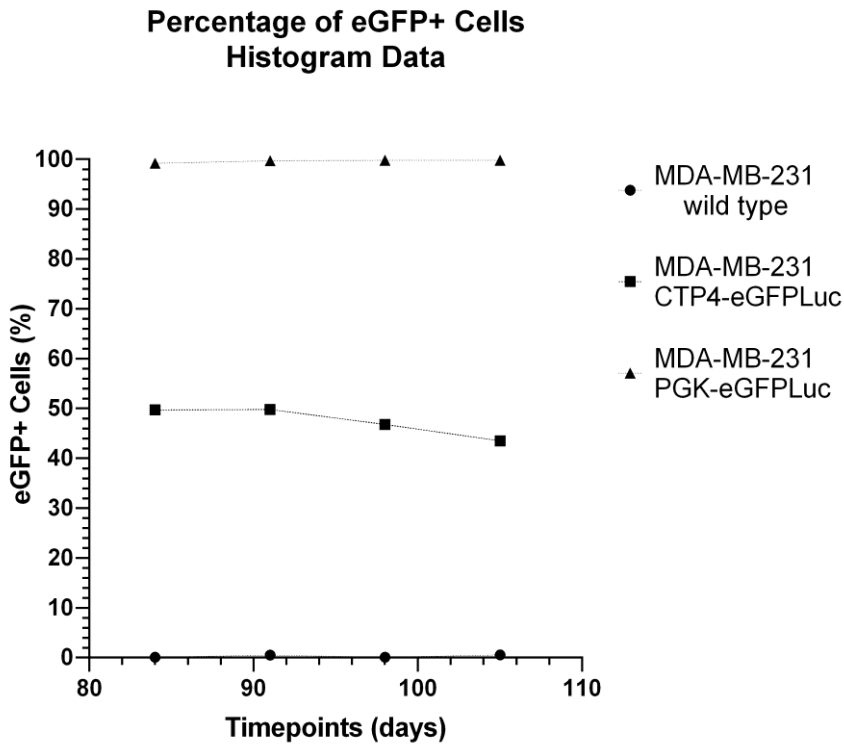
Percentage of eGFP+ Cells
Histogram Data
eGFP+ Cells (%)
100
90
80
70
60
50
40
30
20
10
0
80
90
100
110
Timepoints (days)
MDA-MB-231
wild type
MDA-MB-231
CTP4-eGFPLuc
MDA-MB-231
PGK-eGFPLuc

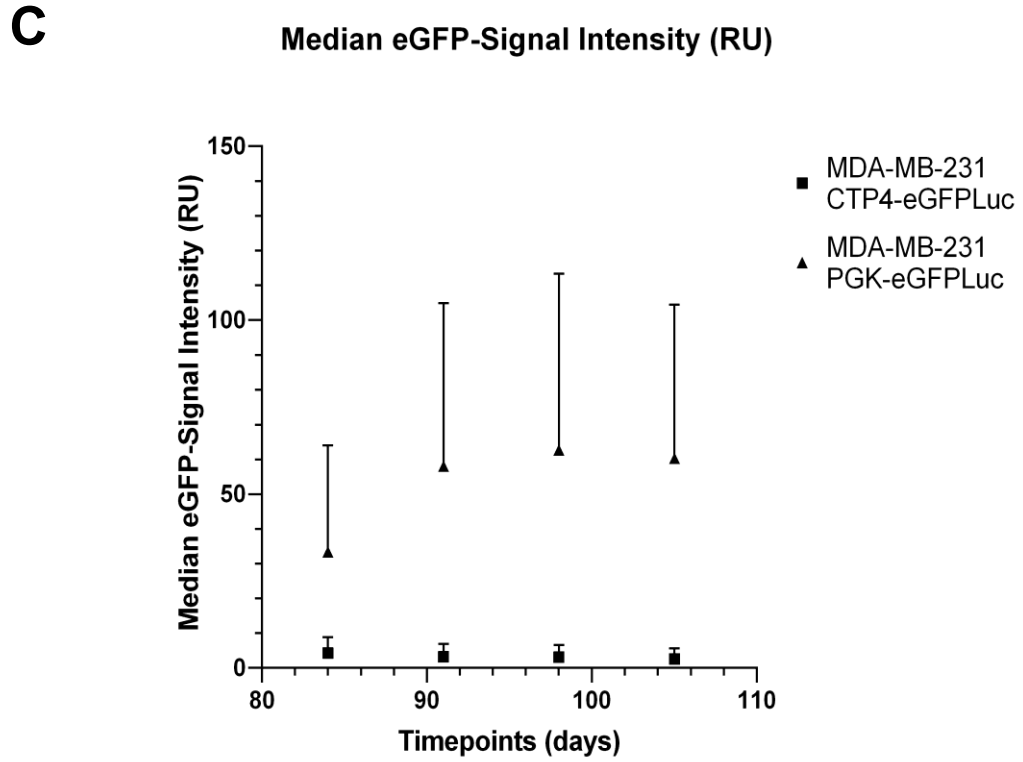

Figure 10. Flow cytometry measurements for MDA-MB-231 wild type, MDA-MB-231 CTP4-eGFPLuc, and MDA-MB-231 PGK-eGFPLuc of newly thawed cells. The cells frozen as the back-up plan with passage numbers identical to the day 84 of the main measurement were thawed up, cultured onward, and measured in the same time intervals**.** A) The percentage of eGFP+ cells based on B1-A/B3-A-plot data. B) The percentage of eGFP+ cells based on B1-A-histrogram data. C) The median eGFP-signal intensity per eGFP+ cell calculated by FlowJo®. Error bars represent the standard deviation from approximately 10,000 measured cells. A) and B) Data represent one measurement per condition on respective days.

Another set of experiments with newly thawed MDA-MB-231 CTP4-eGFPLuc and MDA-MB-231 PGK-eGFPLuc cells, with passage numbers same as on days 84-105 of the first experiment, was done in order to confirm the findings of the first experiment.

The results of measurements with newly thawed MDA-MB-231 PGK-eGFPLuc, with passage numbers same as on days 84-105 of the first experiment (Figures 10A, B and C) are consistent with the observations from the first experiment. This allows again to conclude that no gene silencing of this insert has occurred in this period. The values of the median eGFP-signal intensities are slightly higher compared to the values

obtained in the first experiment, but in the same range (Figure 10C). This is estimated to be in a normal biological range of variation.

The results of measurements with newly thawed MDA-MB-231 CTP4-eGFPLuc with passage numbers same as on days 84-105 of the first experiment differ slightly from the results of the first experiment (Figures 10A, B and C). The percentage of eGFP+ cells starts at slightly lower values than at the same timepoint in the first experiment, and also shows a slight decrease at the following timepoints (Figures 10A and B). However, due to the heterogeneity of this lentivirally transduced cell line subtype, the fact that the percentage of eGFP-expressive cells depends on the activeness of Wnt pathway, different proliferation rates for live-cell material and the lack of further measurements, the underlying cause cannot unequivocally be established.

4.2. Establishment of homogeneous cell line subtypes originating from a single cell

Lentiviruses have proven their usefulness as very efficient gene delivery systems (Zufferey et al. 1998), However, the exact gene insert spot in host cell DNA, and related to this, the possible insert silencing, as well as the number of gene inserts per individual cell, are not subjected to control (Berry et al. 2006; Emery et al. 2002; Charrier et al. 2011). All this leads to creation of very heterogeneous cell line subtypes via lentiviral transductions.

In this experiment, we aimed to establish homogeneous cell line subtypes originating from one single cell, by application of an extremely sparse seeding approach. In this process, we observed several interesting characteristics.

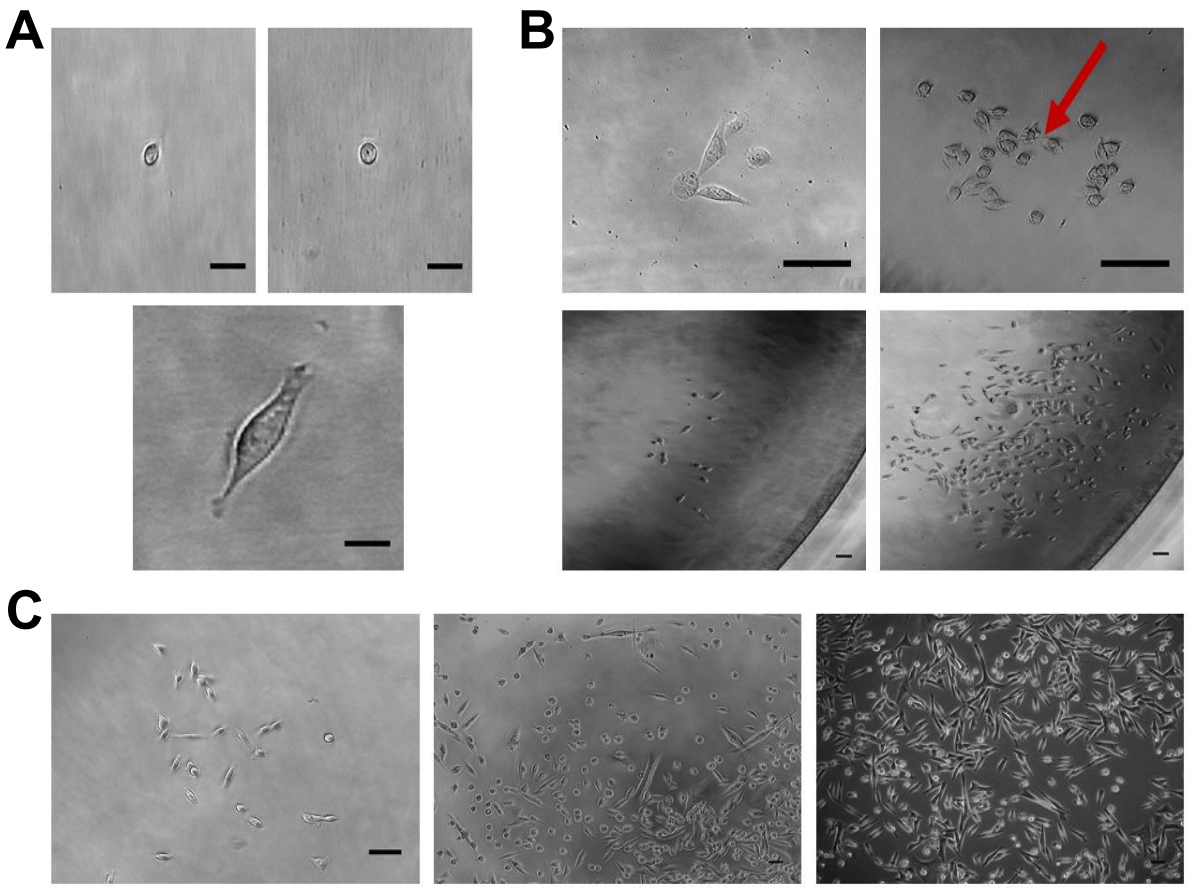

Figure 11. Single cell culture of MDA-MB-231 CTP4-eGFPLuc and MDA-MB-231 PGK-eGFPLuc. A) Initial seeding of MDA-MB-231 CTP4-eGFPLuc. The pictures in the first row were taken immediately after the seeding and illustrate the similarity between the round-shaped cell (left picture) and the cell-like structure or cell in the process of dying off (right picture). The picture in the second row was taken in the morning after the seeding, at which point the cell has already attached to the bottom, and has taken its normal, elongated form. B) In the first row, initial colony generated from isolated single cell of MDA-MB-231 PGK-eGFPLuc exhibiting slow growth after a week from initial seeding (left picture) and dying off of the cells (right picture, red arrow marks dying cells) are shown. In the second row, the same well of a MDA-MB-231 PGK-eGFPLuc single cell generated colony after one week of growth (left picture) and two weeks of growth (right picture) is shown. C) The genesis of a homogeneous cell line subtype originating from an isolated MDA-MB-231 CTP4-eGFPLuc single cell. Left picture is taken after one week of growth in a 96 well plate, and middle picture after three weeks of growth in a 96 well plate. Cells were finally confluent enough for the transfer into a larger well format. The right picture shows the cells reaching 90% confluency in a 25cm² tissue culture flask after 7 weeks of culturing. The scale bar is set at 50µm.

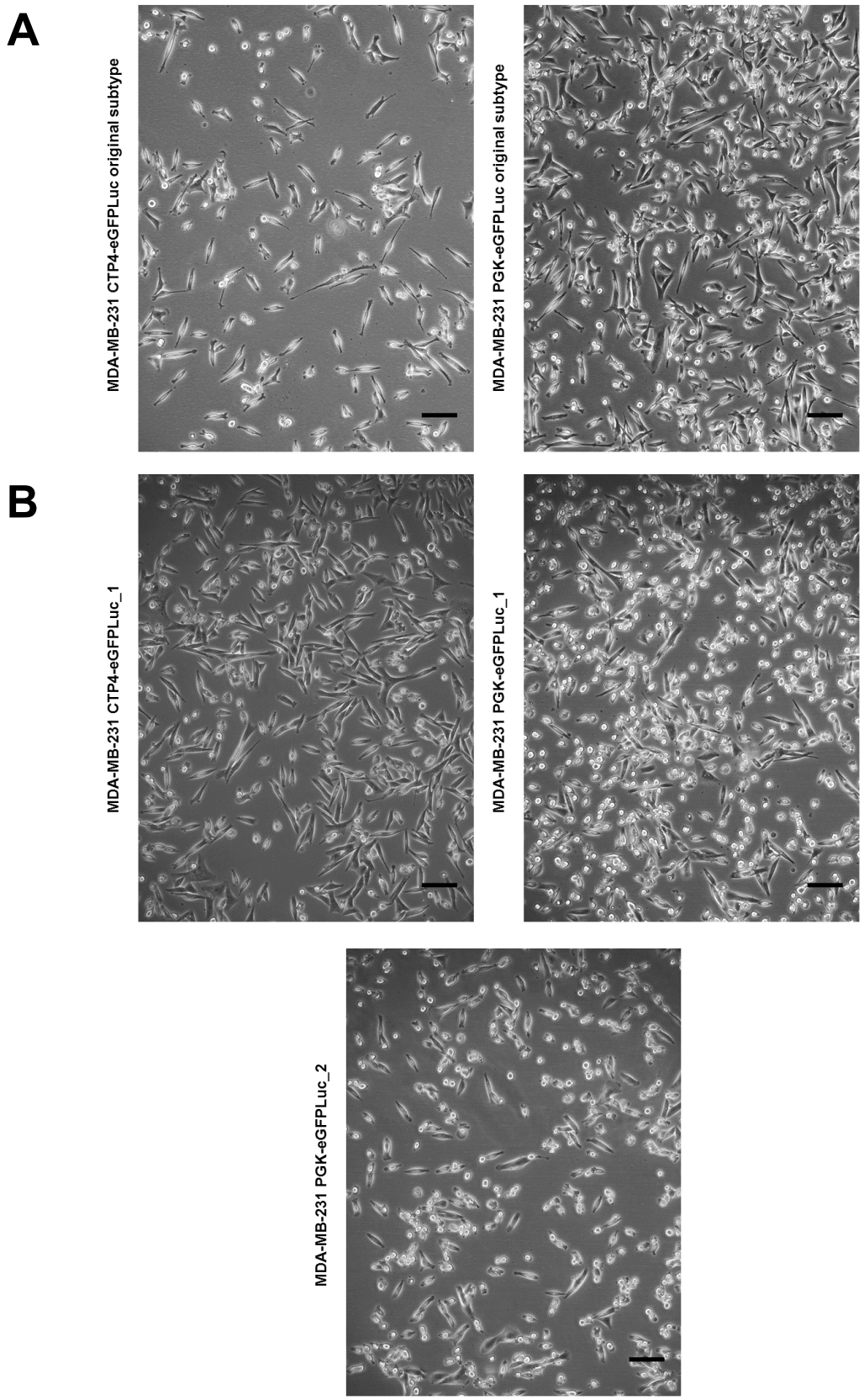

Figure 12. Morphology of SCC-generated cell line subtypes and the original cell lines. A) Large diversity in morphology between individual cells within original cell line subtypes is present. B) In

contrast, all cells among one newly created cell line subtype were morphologically similar. The scale bar is set at 100µm.

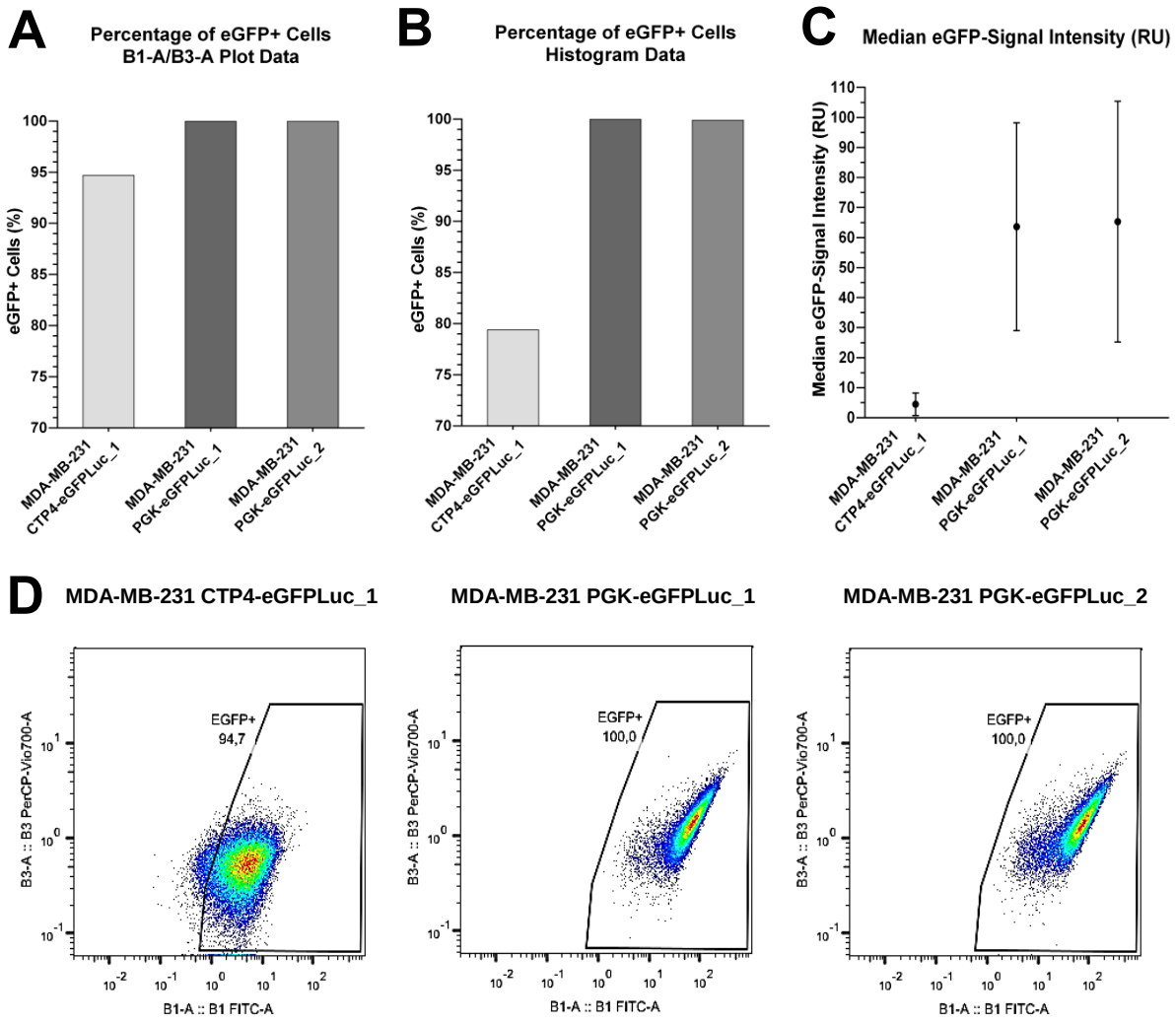

Figure 13. The results of flow cytometry measurements for the SCC-generated cell line subtypes, MDA-MB-231 CTP4-eGFPLuc_1, MDA-MB-231 PGK-eGFPLuc_1 and MDA-MB-231 PGK-eGFPLuc_2. A) The percentage of eGFP+ cells based on B1-A/B3-A-plot data. B) The percentage of eGFP+ cells based on B1-A-histrogram data. C) The median eGFP-signal intensity per eGFP+ cell calculated by FlowJo®. Error bars represent the standard deviation from approximately 10,000 measured cells. D) B1-A/B3-A plots of the respective SCC-generated cell line subtypes. Same gating strategy described in detail in Figure 5. was applied here for data set evaluation. A) and B) Data represent one measurement per condition.

In the hours immediately after the initial seeding, cells were round and not attached to the well bottom, which made them more difficult to spot (Figure 11A, first row). In the morning after the seeding, cells were attached to the well bottom in their characteristic elongated shape, but still not dividing, making this an ideal point for the start of observation (Figure 11A, second row).

Directly after the first cell division, cells showed no tendency to migrate. In fact, they stayed very close to the original cell and divided further there (Figure 11B). This initial cell division was very slow, e.g. it took them approximately 3 weeks to reach 90% confluency in a 96 well plate (Figure 11C, middle picture). Due to the clustering of cells in certain region of the well, cells started to die off (Figure 11B, first row right picture), which is why they subsequently were gently detached and evenly spread every time medium was exchanged.

The cells of the SCC-generated cell line subtype MDA-MB-231 CTP4-eGFPLuc_1 show morphological similarity to one another (Figure 12B), which is in contrast to morphological diversity among the cells of the original MDA-MB-231 CTP4-eGFPLuc (Figure 12A). Also, the cells of the SCC-generated cell line subtype MDA-MB-231 PGK-eGFPLuc_1 show morphological similarity to one another (Figure 12B), which is in contrast to morphological diversity among the cells of the original cell line subtype MDA-MB-231 PGK-eGFPLuc (Figure 12A). Same applies to the cells of the SCC-generated cell line subtype MDA-MB-231 PGK-eGFPLuc_2 (Figure 12A and B). When comparing those two newly generated MDA-MB-231 PGK-eGFPLuc subtypes strong difference in morphology is visible, even though they originate from the same original cell line subtype (Figure 12B, “MDA-MB-231 PGK-eGFPLuc_1” vs. “MDA-MB-231 PGK-eGFPLuc_2”).

After the successful establishment of three single cell culture-generated cell line subtypes, they were analyzed regarding the percentage of the cells expressing eGFP, and the intensity of the eGFP signal per eGFP+ cell. As expected, both single cell culture-generated MDA-MB-231 PGK-eGFPLuc cell line subtypes had 100% of eGFP+ cells (Figure 13A, B and D “MDA-MB-231 PGK-eGFPLuc_1” and “MDA-MB-231 PGK-eGFPLuc_2”). However, the single cell culture-generated MDA-MB-231 CTP4-eGFPLuc cell line subtype had less than 100% of eGFP+ cells, but still significantly

more than the original cell line subtype (Figure 13A and B vs. Figure 9A and B). The values of median eGFP-signal intensities remained in the same range as the values of the respective original cell line subtypes (Figure 13C vs. Figure 9C). Surprisingly, the standard deviation for all three single cell culture-generated cell line subtypes was still quite high (Figure 13C), which is in contradiction with the expected homogeneity of cell line subtypes originating from a single cell.

4.3. Assessment of key cancer characteristics

4.3.1. Transduced MDA-MB-231 subtypes show reduced ability of anchorage-independent growth

Anchorage-independent growth is the ability to grow without the necessity of attachment onto solid surfaces, and as only transformed cells have this ability it is considered to be one of the most important hallmarks of carcinogenesis by some (Borowicz et al. 2014). According to Borowicz et al. (2014) the soft agar colony formation assay is a well-established and rigorous method for *in vitro* characterization of malignant transformations in cells. It is utilized for observing differences regarding number of created colonies at the endpoint, as well as mean spheroid size, and size distribution among created colonies. Here, we used MCF7 as a luminal epithelial cell line, and MDA-MB-231 wild type as a basal-like epithelial cell line. Additionally, we also compared MDA-MB-231 wild type and the two of its lentivirally transduced subtypes.

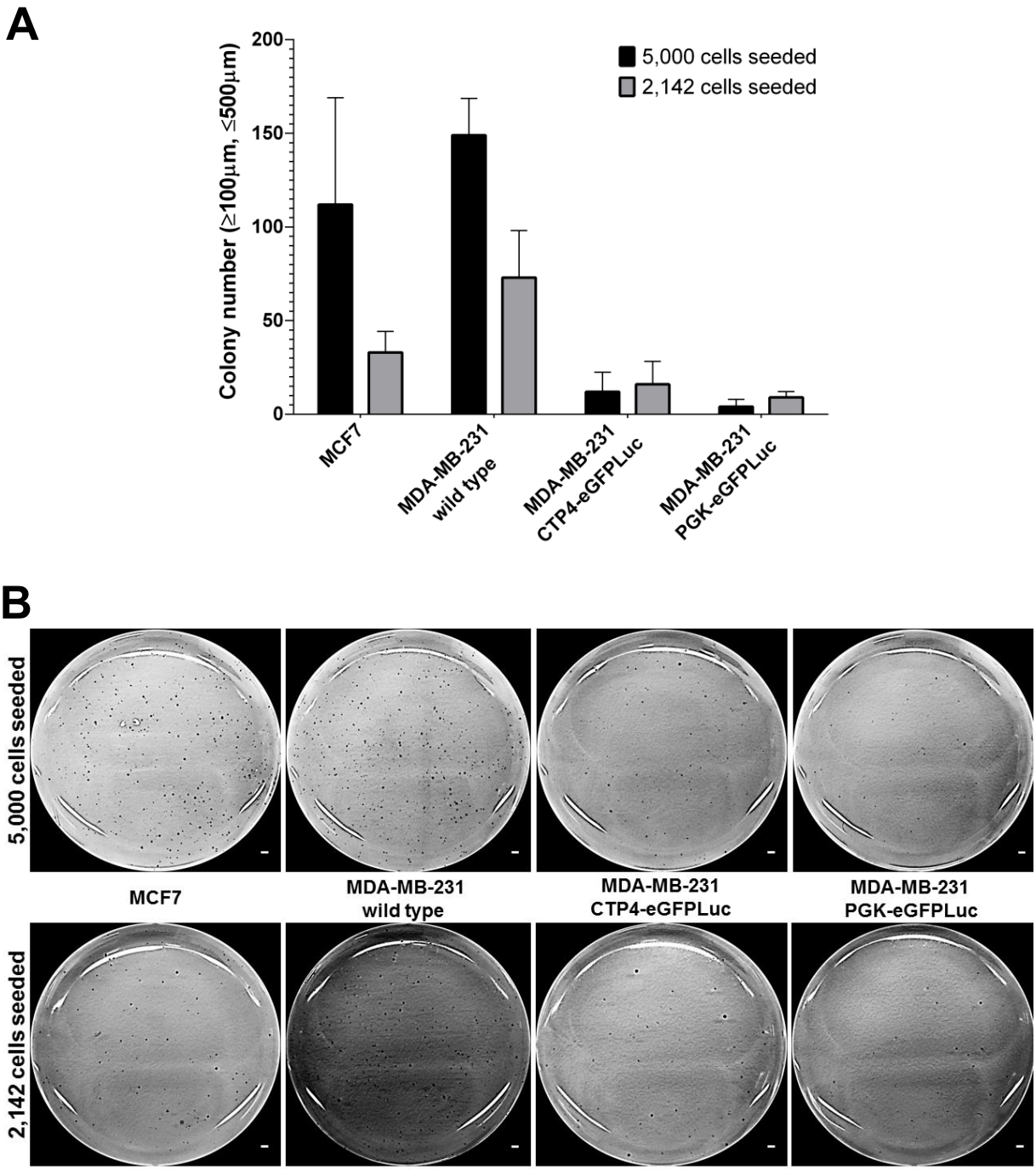

Figure 14. Results of both soft agar colony formation assays performed with MCF7, MDA-MB-231 wild type, MDA-MB-231 CTP4-eGFPLuc, and MDA-MB-231 PGK-eGFPLuc, once with 5,000, and once with 2,142 cells seeded. A) Total number of colonies grown at endpoint of 21 days with a diameter bigger than or equal to 100µm and smaller than or equal to 500µm. Each condition was performed in triplicates. Error bars represent the standard deviation. The process of counting and size exclusion was done in ImageJ® as described in Figure 7. B) Pictures of representative wells taken with the camera at endpoint for each cell line with both 2,142 and 5,000 cells seeded, and adjusted for sharpness/brightness/contrast in PowerPoint (Microsoft® Office 2016). Scale bar is set to 1,000µm.

A

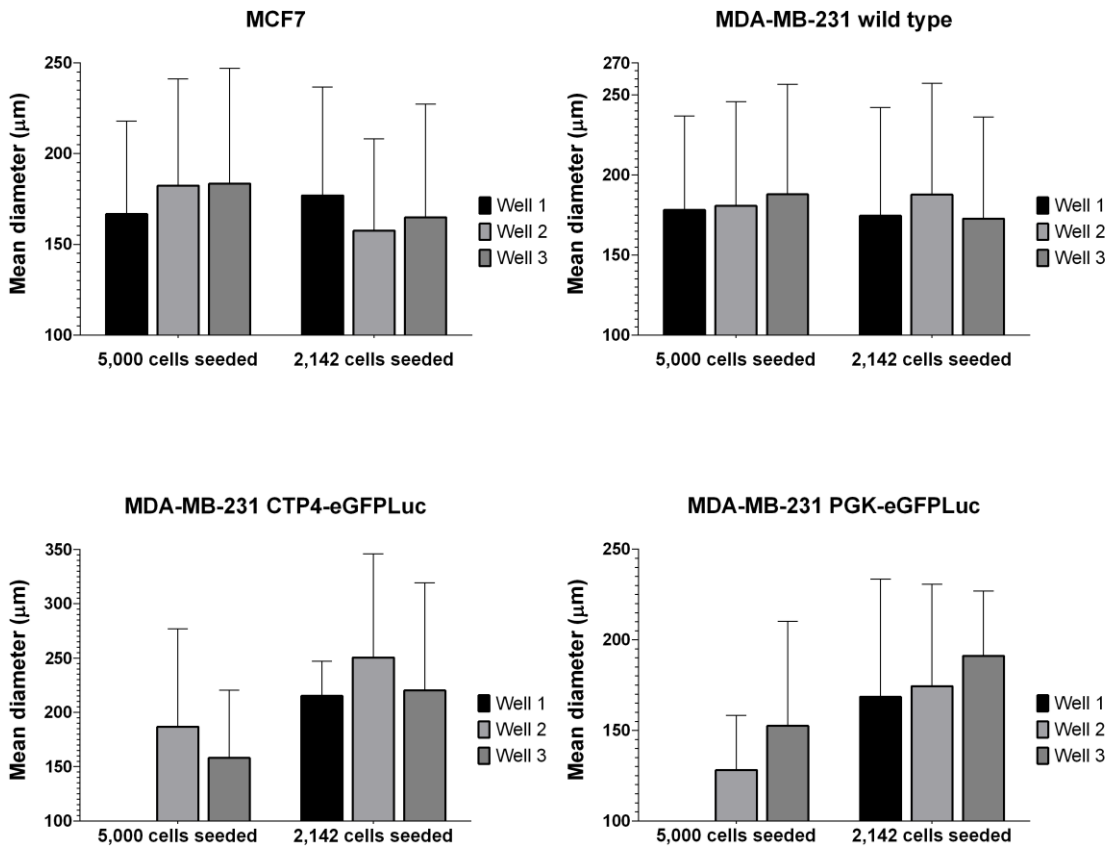

B

			100 µm - 199 µm	200 µm - 299 µm	300 µm - 399 µm	400 µm - 499 µm	Total
MCF7	5,000 cells seeded	Well 1	39	9	1	0	**49**
		Well 2	110	44	6	0	**160**
		Well 3	81	41	4	1	**127**
	2,142 cells seeded	Well 1	21	7	1	0	**29**
		Well 2	22	2	1	0	**25**
		Well 3	34	11	0	1	**46**
MDA-MB-231 wild type	5,000 cells seeded	Well 1	112	33	12	0	**157**
		Well 2	11	46	6	1	**164**
		Well 3	85	33	8	1	**127**
	2,142 cells seeded	Well 1	39	9	3	1	**52**
		Well 2	43	16	8	0	**67**
		Well 3	75	22	2	2	**101**
MDA-MB-231 CTP4-eGFPLuc	5,000 cells seeded	Well 1	0	0	0	0	**0**
		Well 2	11	2	1	1	**15**
		Well 3	16	3	1	0	**20**
	2,142 cells seeded	Well 1	1	2	0	0	**3**
		Well 2	7	8	2	2	**19**
		Well 3	14	7	4	2	**27**
MDA-MB-231 PGK-eGFPLuc	5,000 cells seeded	Well 1	0	0	0	0	**0**
		Well 2	8	0	0	0	**8**
		Well 3	4	1	0	0	**5**
	2,142 cells seeded	Well 1	8	3	1	0	**12**
		Well 2	6	4	0	0	**10**
		Well 3	4	2	0	0	**6**

Figure 15. Results of both soft agar colony formation assays performed with MCF7, MDA-MB-231 wild type, MDA-MB-231 CTP4-eGFPLuc, and MDA-MB-231 PGK-eGFPLuc, once with 5,000, and once with 2,142 cells seeded. A) The calculated mean diameters in µm for each cell type and

each well separately in both experiments. The calculations were done in Excel (Microsoft® Office 2016) based on area surface data acquired from ImageJ®. Error bars represent the standard deviation (SD) of the diameters. Number of replicates and SD values were as follows: n = 49 + 51.3µm, n = 160 + 58.8µm, n = 127 + 63.6µm, n = 29 + 59.8µm, n = 25 + 50.5µm, n = 46 + 62.4µm ("MCF7"), n = 157 + 58.7µm, n = 164 + 65.0µm, n = 127 + 68.8µm, n = 52 + 67.7µm, n = 67 + 69.5µm, n = 101 + 63.6µm ("MDA-MB-231 wild type"), n = 0 + 0.0µm, n = 15 + 90.1µm, n = 20 + 62.4µm, n = 3 + 31.9µm, n = 19 + 95.2µm, n = 27 + 99.1µm ("MDA-MB-231 CTP4-eGFPLuc"), n = 0 + 0.0µm, n = 8 + 30.2µm, n = 5 + 57.8µm, n = 12 + 65.1µm, n = 10 + 56.2µm, n = 6 + 35.8µm ("MDA-MB-231 PGK-eGFPLuc"). B) The spheroid size distribution based on data acquired from calculations previously done in Excel for each cell type and in both experiments separately.

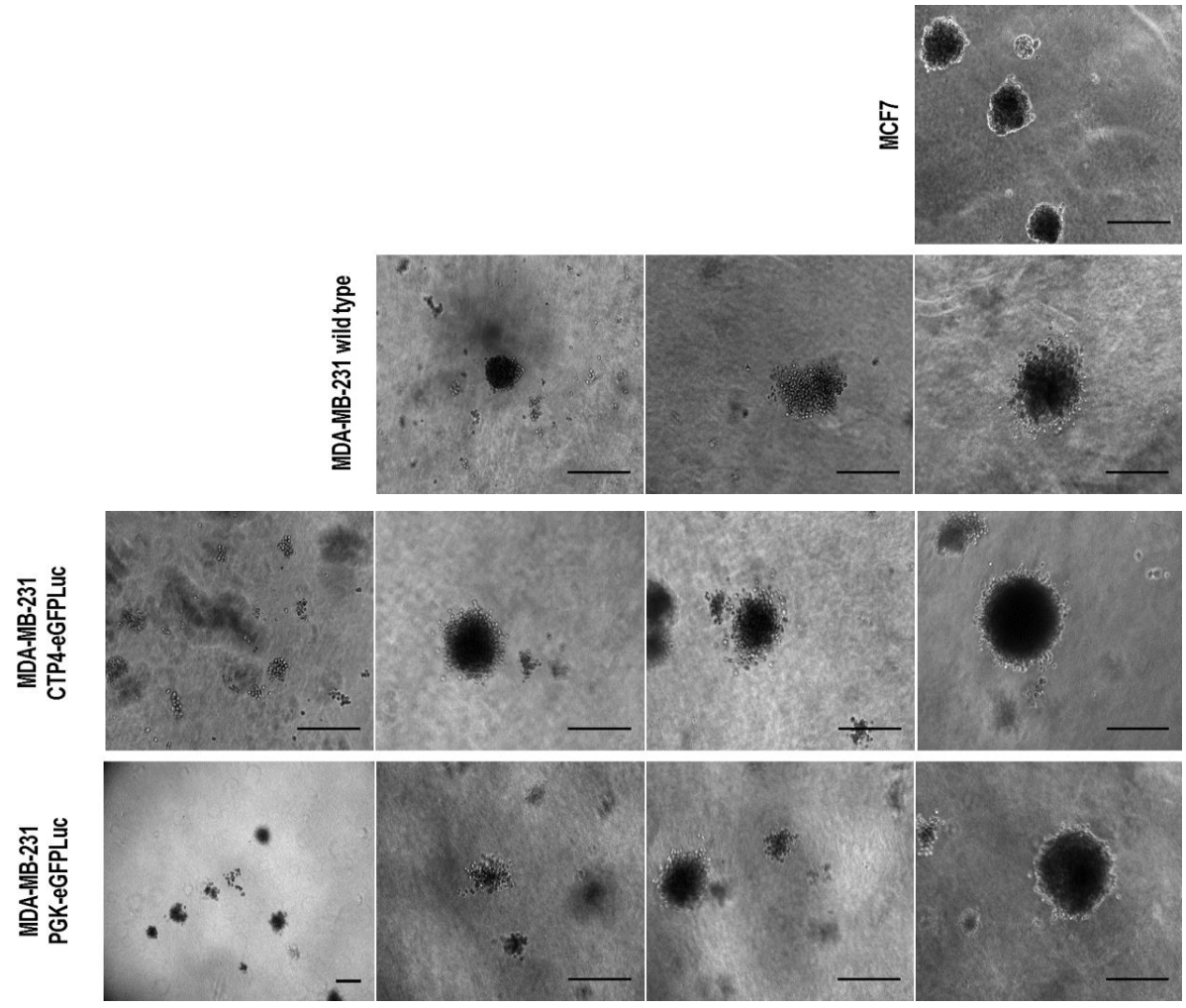

Figure 16. Microscopy pictures of representative spheroids for each cell type at endpoint. The difference between the compact spheroids of the luminal epithelial cell type MCF7 and rather loose aggregates of the basal-like epithelial cell type MDA-MB-231 and its subtypes is clearly visible. Also, the high variation in sizes from very small colonies (upmost left) to very large colonies (upmost right) is clearly visible. Scale bar is set to 300µm.

We here considered only colonies with a diameter ranging from 100µm-500µm as spheroids. At the 21-day endpoint, basal-like epithelial cell line MDA-MB-231 wild type demonstrated an increased ability of anchorage-independent spheroid formation in comparison to the luminal epithelial cell line MCF7 in both experiments (Figure 14A and 14B). Both of the MDA-MB-231 transduced cell line subtypes exhibited a strongly decreased ability to form spheroids in anchorage-independent conditions in comparison to the wild type cell line in both experiments (Figure 14A and 14B).

Regarding the mean spheroid diameter at the endpoint, the majority of wells presented mean diameters in the range between 150µm and 200µm, extended by the standard deviation values to the diameter range between 100µm and 250µm for all cell types (Figure 15A). More detailed analysis revealed that the sizes of the most of the counted spheroids were distributed in the range between 100µm and 299µm, and only a smaller proportion of them was distributed in the size range between 300µm and 500µm (Figure 15B). The additional up-close observation under the light microscope confirmed this high variation in spheroid sizes for all cell types (Figure 16). It also confirmed that MCF7 is prone to build compact spheroids, whereas MDA-MB-231 and its subtypes are rather prone to build loose aggregates (Figure 16).

4.3.2. Transduced MDA-MB-231 subtypes show no changes in migratory ability

Malignant cancer can make use of their intrinsic migratory ability to invade to adjacent tissues and the vasculature, and ultimately to metastasize to distant sites (Yamaguchi and Condeelis 2007). The ability to activate invasion and metastasis is one of *the six hallmarks of cancer* (Hanahan and Weinberg 2011). Since the scratch assay partly imitates *in vivo* cell migration process, it is considered to be a simple *in*

vitro method for the studying of migratory ability of cell types (Liang, Park, and Guan 2007).

The scratch assay was utilized to examine whether there are any changes in migratory ability in MDA-MB-231 cell line due to lentiviral transductions. The migratory abilities of MDA-MB-231 CTP4-eGFPLuc and MDA-MB-231 PGK-eGFPLuc were compared to the migratory ability of MDA-MB-231 wild type at several time points in two experiments, with different starvation approaches. Shortly, a scratch is made in a confluent cell layer, in which the cells will migrate back again over time (Figure 17A). The migratory ability is determined by calculating open wound areas at given timepoints, and setting them in a relation to the original open wound area directly after the scratch.

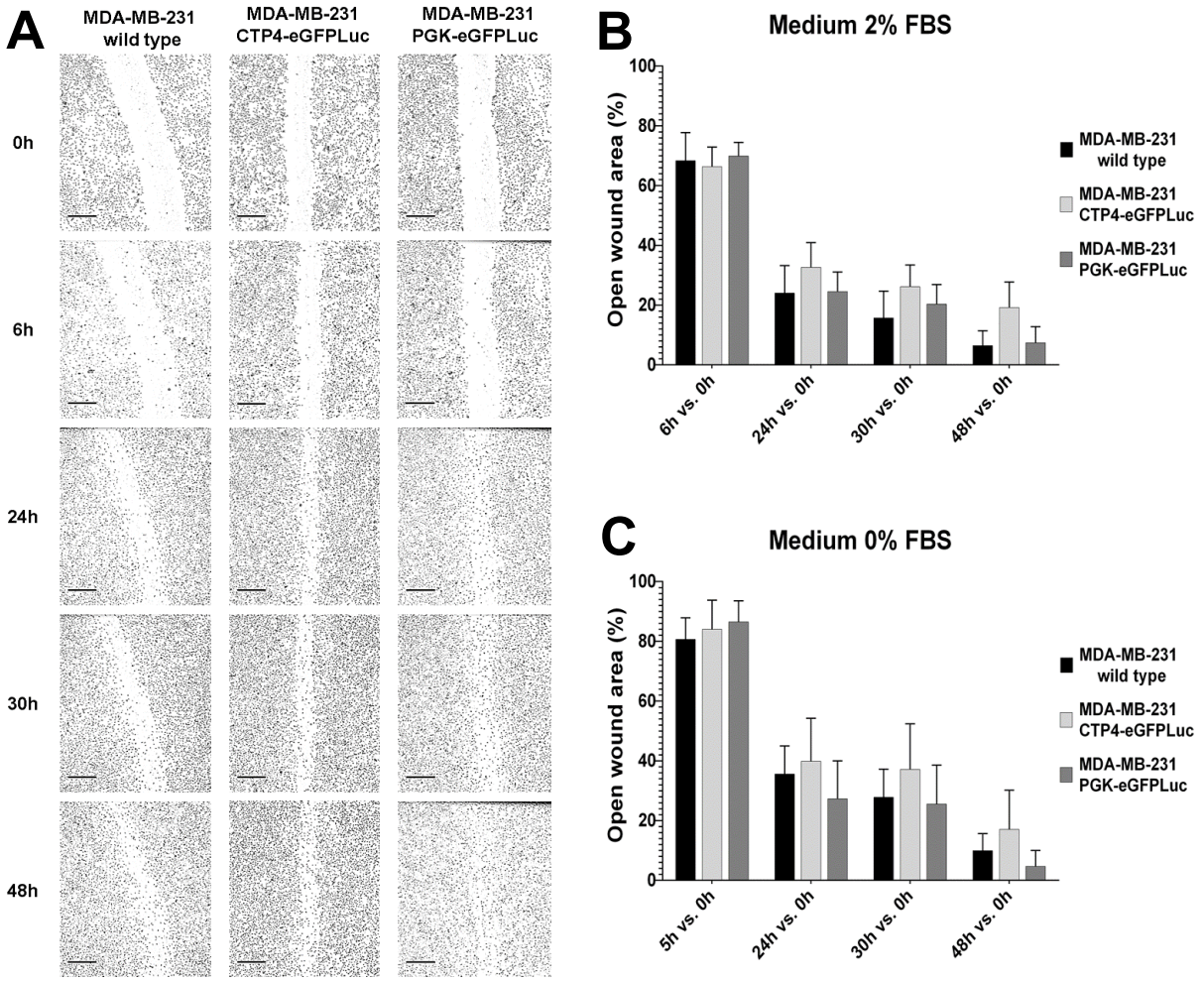

Figure 17. Scratch assays reveal similar migratory potential in MDA-MB-231 wild type, MDA-MB-

231 CTP4-eGFPLuc, and MDA-MB-231 PGK-eGFPLuc. A) Representative pictures of scratches for each cell type at timepoints 0h, 6h, 24h, 30h, and 48h. Pictures were taken with EVOS® FL Imaging System with 4x objective, and adjusted for sharpness/brightness/contrast in PowerPoint (Microsoft® Office 2016). Scale bar is set to 400µm. B) Percentage of open wound area in medium with 2% FBS administered in the night prior to scratch. This reduced FBS medium was kept for the full remaining experiment duration., in contrast to C) an approach where we administered medium with 0% FBS for 24 hours before scratch, then immediate to scratch infliction the normal culture conditions were restored and kept until the end of experiment. B) Number of replicates were as follows: n = 18 for MDA-MB-231 wild type, n = 14 for MDA-MB-231 CTP4-eGFPLuc and n = 13 for MDA-MB-231 PGK-eGFPLuc. C) Number of replicates were as follows: n = 11 for MDA-MB-231 wild type, n = 9 for MDA-MB-231 CTP4-eGFPLuc and n = 10 for MDA-MB-231 PGK-eGFPLuc.

Both experiments indicate comparable wound closure between the three cell types tested, leading us to conclude that there was no significant change in migratory ability in MDA-MB-231 CTP4-eGFPLuc and MDA-MB-231 PGK-eGFPLuc due to transductions (Figure 17B and C).

4.4. Soft agar colony formation assay in combination with single cell culture

In order to observe anchorage-independent growth of a spheroid originating from a single cell over time, an assay that combines soft agar colony formation assay with single cell culture method in 96 well plate was designed. This assay has proven to be an effective method for 2D and 3D imaging of MDA-MB-231 PGK-eGFPLuc spheroids and their growth over time.

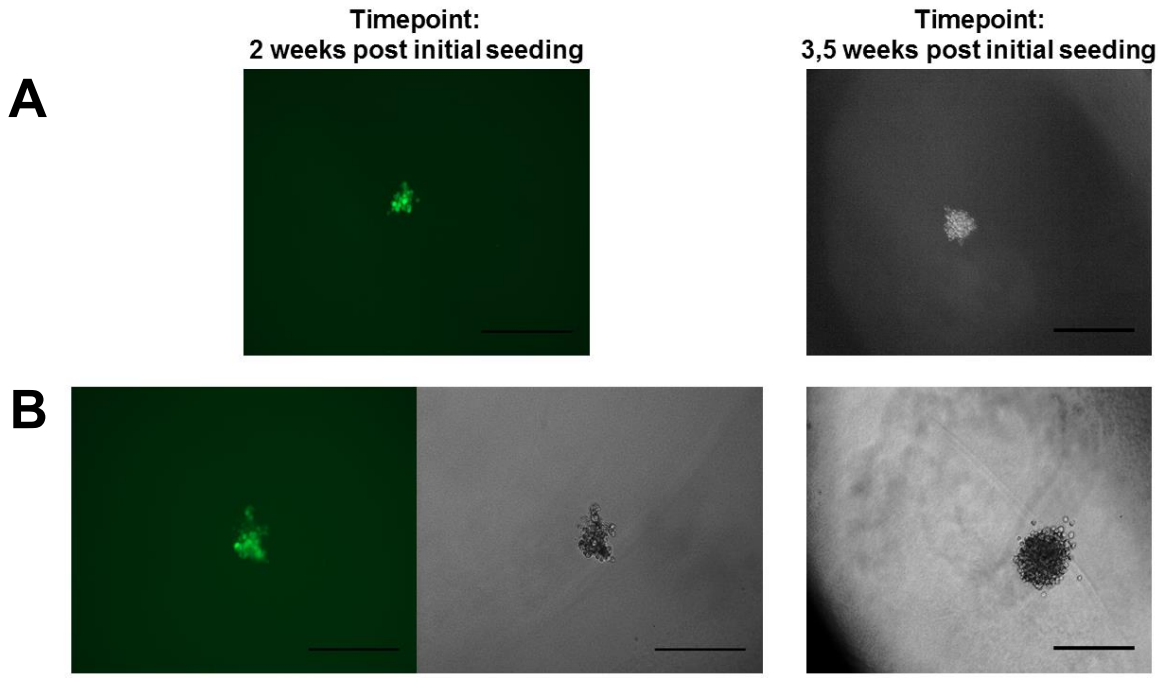

Figure 18. Growth monitoring of same spheroids in soft agar over time in 96 well plate. Cell line used here is MDA-MB-231 PGK-eGFPLuc subtype. Left and middle pictures show spheroids A and B 2 weeks after seeding and right pictures same spheroids 3,5 weeks after seeding. Images were taken with 10x objectives EVOS® FL Imaging System (left and middle pictures, whereas left pictures represent eGFP-fluorescence signal) and Motic AE31 series Microscope Moticam 3.0MP (right pictures). Brightness/contrast were adjusted when needed. The scale bar is set at 300µm.

In this try-out experiment, out of 300 single cells seeded in total, only 6 spheroids in 6 separate wells were gained and their growth was observed over time. In this assay, cells float in soft agar, dispersed in a 3D-stack, while in conventional single cell seeding, cells attach and can be imaged in one plane, namely at the well bottom. This made the process of finding single cells on the morning after the seeding very difficult. On top of this, small soft agar particles were interfering with the imaging process. As such, first spheroids were first scored 2 weeks post initial seeding, and their growth was observed only from this point onwards (Figure 18).

4.5. Methyl cellulose assay yields fragile aggregates in MDA-MB-231 cells and subtypes

The methyl cellulose assay is used to obtain aggregates in a significantly faster manner (Bilandzic and Stenvers 2014) compared to the soft agar colony formation assay. Aggregates obtained with this assay are actually clusters of, in this case, all 3,000 seeded cells, that are spun down. This means that these represent multicellular aggregates created artificially and, in contrast to a single cell grown spheroid, consist e.g. out of non-genetically uniform cells (Bilandzic and Stenvers 2014). Due to the fast aggregate formation, however, an easy and fast aggregate retrieval should be possible, making this assay an useful source of aggregates for novel downstream methods such as histological cryosectioning.

In this try-out-experiment, we aimed to characterize loose aggregates of basal-like epithelial cell line MDA-MB-231 and its subtypes obtained by methyl cellulose assay in regard to their shape and size. Furthermore, we aimed to examine if this method can be used to obtain and retrieve those aggregates for downstream applications, such as cryosectioning. As a comparison, we also used MCF7 cells, which were assumed to create more compact aggregates.

As expected, very compact aggregates were obtained with MCF7 (Figure 19A “MCF7”). Even after several pipetting steps, and after the actual harvesting, those aggregates remained compact (Figures 19B and 19C ”MCF7”). However, as anticipated, MDA-MB-231 and its subtypes formed loose aggregates (Figure 19A). Already after one pipetting step, these aggregates fell mostly apart (Figure 19B). This suggested that the harvesting is likely to damage aggregates generated in this cell line, a fact that we later confirmed (Figure 19C “MDA-MB-231 wild type”, “MDA-MB-231 CTP4-eGFPLuc” and “MDA-MB-231 PGK-eGFPLuc”). Interestingly, MDA-MB-231 CTP4-eGFPLuc aggregates were even less compact than MDA-MB-231 wild type aggregates, exhibiting occasional holes in their inner structure (Figure 19A “MDA-MB-231 CTP4-eGFPLuc”).

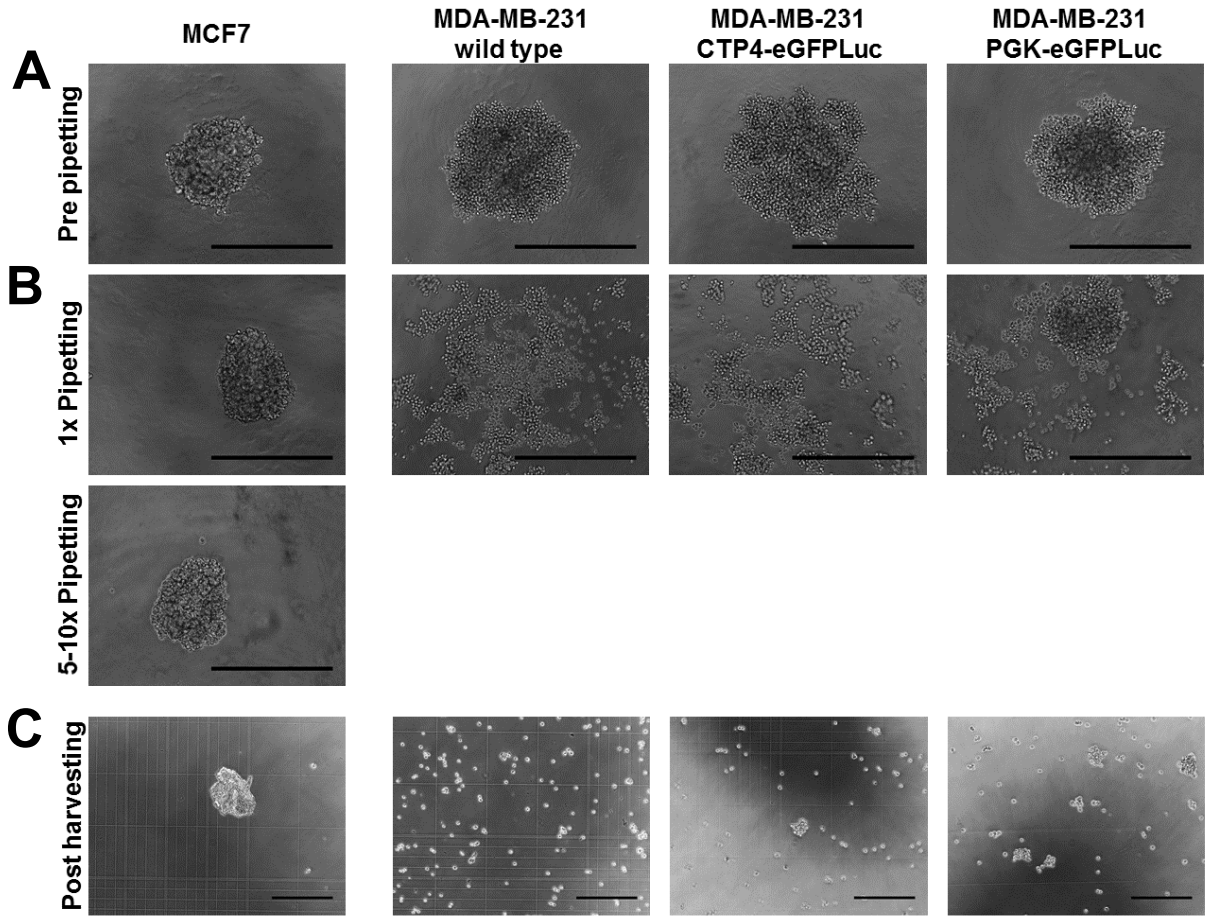

Figure 19. Characterization of MCF7 (leftmost column), MDA-MB-231 wild type (middle left column), MDA-MB-231 CTP4-eGFPLuc (middle right column), and MDA-MB-231 PGK-eGFPLuc (rightmost column) multicellular aggregates obtained by methyl cellulose assay. A) Pictures taken 24 hours after generation but prior to harvesting to determine size and shape of generated multicellular aggregates. B) Pictures taken after pipetting the same aggregates from Figure 3A) once (first row) or for 5-10 times up and down with 200µl pipette tip (second row) to test if harvesting could work for the cell lines used here. C) After the actual harvesting 10µl of aggregate suspension were transferred in Neubauer chamber and observed without coverslips to assess multicellular aggregates. Images were taken with 10x (C) and 20x (A and B) objective (Motic® AE31 series Microscope with Moticam 3.0MP camera) and sizes were determined in ImageJ®. The scale bar is set at 300µm.

Size measurements of 3 representative wells for each cell type characterized MCF7 aggregates as the smallest, with the mean diameter 229µm ± 9.7µm. Among the MDA-MB-231 cell types, MDA-MB-231 CTP4-eGFPLuc aggregates were characterized as the biggest, with the mean diameter 342µm ± 9.6µm, followed by MDA-MB-231 aggregates with the mean diameter 308µm ± 4.8µm as the middle ones,

and MDA-MB-231 PGK-eGFPLuc aggregates with the mean diameter 285μm ± 26.3μm as the smallest ones.

5. Discussion

The overall aim of this work was to characterize the two newly created MDA-MB-231 human breast cancer cell line subtypes, which were gained via lentiviral insertions of two different reporter gene inserts, namely CTP4-eGFPLuc and PGK-eGFPLuc.

In the first part of this work, we focused on the assessment of the long-term expression stability of the two lentivirally inserted transgenes and on the assessment of the activities of the respective promoters via flow cytometry, as to our knowledge this was never done before with this human breast cancer cell line.

As mentioned in the introduction of this work, lentiviral gene inserts are susceptible to *chromosomal position effects* and in this relation to the possibility of high expression variegation or gene silencing (Emery et al. 2002). Our data for lentiviral PGK-eGFPLuc inserts showed both continuously high expression levels as well as consistency in expression intensities, which were also confirmed in the second-round measurements. As the constitutive promoter-eGFP is expected to be expressed in all cells with the gene casette (Norrman et al. 2010), this led to definite conclusion of long-term expression stability for lentiviral PGK-eGFPLuc inserts in MDA-MB-231 cell line. Moreover, our results are in concordance with the results of Ramezani et al. (2000), in which long-term expression stability of lentiviral PGK-eGFP inserts in human hematopoietic cells KG1a was described.

In contrast, our data for lentiviral CTP4-eGFPLuc inserts showed variegation in expression levels but consistency in expression intensities, which were also confirmed in the second-round measurements. However, since CTP4 is classified as a Wnt pathway-dependent promoter with measurable expression only in cells with deregulation in this pathway (Lipinski et al. 2004), and both due to the expected heterogeneity mirroring the variable proviral transgene integration number (Charrier et al. 2011) in combination with different proliferation rates for live-cell material, as well as due to the lack of measurement possibilities in the present population with normal Wnt pathway regulation, no definite conclusions on long-term expression stability of

lentiviral CTP4-eGFPLuc inserts in MDA-MB-231 cell line are possible based on our data.

eGFP-expression-level data was calculated by two different gating approaches for eGFP+ cells in parallel, in order to compare the two (Figure 20A vs. Figure 20B). The second gating approach, on the basis of B1-A-histogram for data display (Figure 20B), is widely used in many scientific papers utilizing the measurements of GFP expression levels (Pannell et al. 2000; Yao et al. 2004; Katz et al. 2007). However, when displaying the data on histogram the origin of the fluorescence is not taken into full account, since it does not offer the possibility to gate around autofluorescent cells, as it is the case when displaying the data on B1-A/B3-A-plot (Figure 20). Subsequently, this leads either to false-negative populations, whose effects in our case are especially visible when gating for eGFP+ cells on histogram in MDA-MB-231 CTP4-eGFPLuc cells (Figure 20, middle column) or to false-positive populations as it was the case in the work of Li et al. (2012). In conclusion, the gating approach on the basis of B1-A/B3-A-plot as a mean for data display provides more accurate results, as it offers the possibility of accurate fluorescence discrimination in regard to its origin, e.g. gating out of widely present autofluorescent cells.

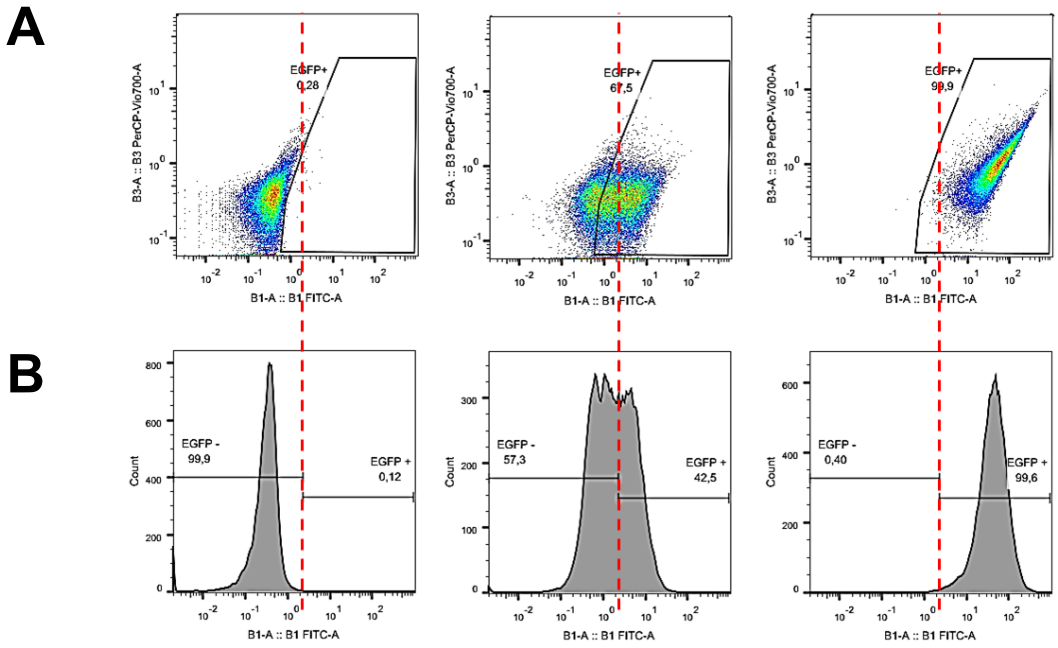

Figure 20. Direct comparison between the two gating strategies utilized for calculations of eGFP-

expression levels in this work. A) The gating strategy on basis of the B1-A/B3-A-plot. B) The gating strategy on basis of the B1-A-histogram. The red lines indicate the exact differences in gated populations between the two strategies. Visualization based on BioLegend® Blog - Flow Cytometry Data Analysis II: Show Your Hidden Data.

Qin et al. (2010) did a systematic activity comparison of constitutive promoters, including PGK promoter in various mammalian cell lines, transduced with promoter of interest and GFP as reporter gene via lentiviral gene delivery systems. In their results, PGK was among the weakest constitutive promoters with mean GFP-signal intensity between 0 and 5,000 depending on cell line used (Qin et al. 2010). However, the MDA-MB-231 cell line was not a part of this extensive comparison, and since the comparison of GFP intensities among different cell types does not reflect a true promoter strength due to variable cell-line-dependable GFP-stability (Qin et al. 2010), and due to the facts that we used eGFP for our measurements and calculated median eGFP-signal intensities the direct comparison of our data in regard to the strength of PGK compared to other constitutive promoters in MDA-MB-231 cell line is not possible. Moreover, the activity of CTP4 promoter was characterized only with non-virally transduced human colon cancer cell lines and by utilizing luciferase gene expression measurements (Gaedtke et al. 2007). Therefore, the only comparison we can do in this case, is the comparison between PGK and CTP4 in MDA-MB-231 cell line based on our data, which revealed that PGK is approximately 15-fold stronger than CTP4 in MDA-MB-231 cell line.

However, the individual signal strengths were strongly variable for both cell subtypes, which is in direct correlation with the expected heterogeneity of cells transduced via lentiviruses (Charrier et al. 2011).

As an additional and very challenging step, we focused on establishing homogeneous cell line subtypes originating from a single cell, for both of the heterogeneous cell line subtypes. We subsequently assessed their morphology and transgene expression patterns. As such, we successfully established 3 new MDA-MB-231 subtypes, two of which were originating from single cells of MDA-MB-231 PGK-eGFPLuc and one was originating from a single cell of MDA-MB-231 CTP4-eGFPLuc.

As expected, the single cell culture-generated cell line subtypes showed a visible difference in morphology in comparison to each other, but all cells among one newly created cell line subtype were morphologically similar, especially in contrast to highly heterogeneous respective original cell line subtypes. Even though the percentage of eGFP+ cells indicated successful creation of very uniform subtypes in respect to their eGFP-expression levels, the analysis of their median eGFP-signal intensities revealed surprisingly still present high standard deviations in same range and as previously described with original cell line subtypes. This is in contradiction with expected homogeneity of cell line subtypes originating from an isolated single cell, but we speculate that those initially isolated single cells had more than one transgene inserts, as commonly acknowledged and highly probable for lentiviral vectors (Charrier et al. 2011), and that additionally one or more of those inserts but never all of them in one particular cell have been subjected to gene silencing, as this variegation with genetically identical sister cells has previously been described by Ellis (2005). Further investigations in this phenomenon would be required.

In the second part of this work, we focused on the assessment of the anchorage-independent growth and migratory ability of the two lentivirally transduced human breast cancer cell line subtypes in comparison to the original cell line. These are considered to be amongst the key cancer characteristics (Borowicz et al. 2014; Hanahan and Weinberg 2000). In addition, the comparison of the growths in anchorage-independent conditions of those basal-like subtypes to MCF7 cell line as a luminal type was performed.

In respect to the mean number of created colonies, the basal-like cell line MDA-MB-231 wild type demonstrated in the two performed experiments 1.5-fold/2.2-fold higher colony-forming potential in comparison to the luminal cell line MCF7, which can be directly interpreted as expected slightly higher *in vivo* tumorigenic potential of basal-like MDA-MB-231 cell line. Results indicating slightly higher colony-forming ability of MDA-MB-231 cells in comparison to MCF7 cells were also acquired indirectly in some studies, where MCF7 and MDA-MB-231 colony numbers were determined as part of a control in experiments with other purposes (Li et al. 2015; ZHAO et al. 2015). In contrast, both lentivirally transduced MDA-MB-231 subtypes demonstrated significant decrease in their mean colony-forming numbers in comparison to MDA-MB-231 wild

type (12.4-fold/4.6-fold for MDA-MB-231 CTP4-eGFPLuc and 37.3-fold/8.1-fold for MDA-MB-231 PGK-eGFPLuc) in both experiments, which can be directly interpreted as expected significantly lower *in vivo* tumorigenic potential or even as possible loss of cancerogenesis due to lentiviral transductions. However, these findings should be also confirmed *in vivo*.

In respect to the size ranges, detailed analysis revealed that most of the counted spheroids were distributed in the range between 100µm and 299µm with no observable differences among the different cell types. We could not find any indications in literature regarding the expected spheroid sizes and their size distribution in the cells we tested. However, microscopy analysis confirmed literature indications (Holliday and Speirs 2011), in which MCF7 cells show tendency of building compact spheroids, whereas MDA-MB-231 cells show tendency of building rather loose aggregates in 3D culture conditions. Additionally, our data show that also lentivirally transduced MDA-MB-231 subtypes show tendency of building rather loose aggregates in 3D culture conditions.

In respect to their migratory ability, we observed comparable wound closure between MDA-MB-231 wild type and its lentivirally transduced subtypes, even with two different starvation approaches we additionally have tested. Thus, compared to MDA-MB-231 wild type no significant change of metastatic potentials in MDA-MB-231 CTP4-eGFPLuc and MDA-MB-231 PGK-eGFPLuc due to transductions is expected *in vivo*.

Serum starvation is a term used for growing cells in either reduced serum, serum-free, or serum- and protein-free medium, as there is no unified protocol to perform this so commonly used procedure (Pirkmajer and Chibalin 2011). Very often, serum starvation is performed in totally serum-free basal medium, or in medium with in relation to normal culture medium low serum concentration, such as 0.05%, 0.1-0.5% or even 2-5% (Pirkmajer and Chibalin 2011). The time duration of serum starvation is also very variable (Pirkmajer and Chibalin 2011). Among many reasons that speak in favour of use of this biological procedure, the (possible) reduction of basal cellular activity (Codeluppi et al. 2011) and cell cycle synchronization due to initiation of cell entering into the quiescent G0/G1 phase (Pontarin et al. 2011) are listed. As in long-term wound healing assays (>24h), the distinction between cell proliferation and

cell motility is not possible (Kramer et al. 2013), we decided to perform two different serum starvation approaches in our experiments. In relation to wound closure both serum starvation approaches we used yielded very similar results. However, in the approach with serum 0% FBS for 24 hours before scratch and restorement of the normal culture conditions immediate to scratch infliction, several scratches needed to be excluded from the analysis due to evident over-confluency of the cell monolayer. Thus, we would recommend the serum starvation approach with medium 2% FBS administration in the night prior to scratch and maintainment of this culture condition for the full remaining experiment duration.

In regard to the two different microscopes and subsequently two different cameras we used for imaging purposes in scratch assay, namely EVOS® FL Imaging System and Motic AE31 series microscope with Moticam 3.0MP, both set of pictures were equally suitable for the evaluation with TScratch software (Gebäck et al. 2009).

In addition to the standard soft agar colony formation assay in non-adherent 6 well plates, we combined this protocol with our protocol for single cell culture in a 96 well plate, which resulted in a challenging assay enabling effective monitoring of the growth of a same spheroid in anchorage-independent conditions. In this first try-out experiment, we managed to generate 6 spheroids in 6 separate wells and follow their growth over time. This experiment would, however, require further optimization, e.g. in order to reach higher output in regard to number of created spheroids, number of seeded cells could be increased.

Lastly, we tested the possibility of utilizing the methyl cellulose assay with MDA-MB-231 cell line and its subtypes, as methyl cellulose assay is utilized to obtain aggregates in a very fast manner (Bilandzic and Stenvers 2014) with the possibility of an easy and fast aggregate retrieval for novel downstream methods such as histological cryosectioning. However, aggregates created in this manner are actually artificial clusters of non-genetically uniform cells (Bilandzic and Stenvers 2014). As indicated in literature (Holliday and Speirs 2011) and confirmed in our soft agar colony formation assays performed with these cell types, very compact aggregates were obtained with luminal MCF7 whereas basal-like MDA-MB-231 and its subtypes formed rather loose aggregates. Furthermore, we anticipated that this rather loose aggregate

structure of MDA-MB-231 and its subtypes might result in ineffective retrieval, which was also confirmed after attempted harvesting. A possible solution would be to include a basement membrane extract (e.g. 2.5% Matrigel™) at the stage of spheroid initiation for improvement of the loose 3D structure (Dale et al. 2014).

In addition, we used this opportunity to characterize the sizes of aggregates consisting of the same number of cells as defined by protocol for methyl cellulose assay. Being the most compact, MCF7 aggregates were characterized as the smallest. Having rather loose structure, MDA-MB-231 aggregates were significantly bigger than MCF7 aggregates. Moreover, MDA-MB-231 CTP4-eGFPLuc aggregates exhibited the loosest structure of the three MDA-MB-231 cells tested with occasional holes in their inner structure, and were thus characterized as the biggest.

Taken together, we were able to conclude the long-term expression stability of lentiviral PGK-eGFPLuc inserts in MDA-MB-231 cell line, but no definite conclusions for lentiviral CTP4-eGFPLuc inserts in MDA-MB-231 cell line were possible based on our data. Furthermore, the assessment of respective promoter activities characterized PGK as approximately 15-fold stronger promoter in comparison to CTP4 in MDA-MB-231 cell line. In addition, we successfully established 3 new MDA-MB-231 subtypes by single cell culture approach, but their transgene expression patterns unexpectedly revealed maintenance of their highly heterogeneous profiles. In terms of key cancer characteristics, our data suggest significantly lower tumorigenic potential or even possible loss of cancerogenesis, but no significant change of metastatic potentials due to lentiviral transductions in MDA-MB-231 human breast cancer cell line. However, these findings should be also confirmed *in vivo*.

6. Appendix

6.1. Abstract

Lentiviral gene delivery systems are widely used for gene delivery, as they show high transduction efficiency, long-term expression stability, and transduction of both dividing and non-dividing cells. However, due to semi-random insertions and integration of variable insert numbers, lentiviral transgenes are also subjected to different epigenetic effects, which can subsequently lead to high variegation in expression or gene silencing. In this work, we characterized the long-term expression stability of lentivirally introduced reporter gene eGFPLuc (a fusion between the fluorescent protein eGFP and the firefly luciferase Luc) under the control of either the constitutive active PGK promoter (PGK-eGFPLuc) or the Wnt pathway-dependent synthetic promoter CTP4 (CTP4-eGFPLuc) in the MDA-MB-231 breast cancer cell line. Based on our measurements, we concluded long-term expression stability of PGK-eGFPLuc inserts in MDA-MB-231 cell line, but no definite conclusions for lentiviral CTP4-eGFPLuc inserts were possible. Furthermore, the assessment of respective promoter activities characterized PGK as approximately 15-fold stronger promoter in comparison to CTP4 in MDA-MB-231 cell line. In addition, we focused on the establishment of homogeneous cell line subtypes originating from a single cell and their transgene expression characterization. In this line, we successfully established 3 new MDA-MB-231 subtypes, but unexpectedly the characterization revealed maintenance of their highly heterogeneous profiles.

In the second part of this work, we compared the lentivirally created sublines to the original MDA-MB-231 human breast cancer cell line, in terms of their tumorigenic (non-adherent colony formation) and metastatic potentials (cell motility) as key cancer characteristics. Two different non-adherent colony formation assays in soft agar and methyl cellulose were applied, and a scratch-wound assay with two different starvation settings. Tumorigenic potential of lentivirally transduced subtypes was significantly reduced, whereas their metastatic potential remained the same. Moreover, the

comparison of basal-like MDA-MB-231 to the luminal breast cancer cell line MCF7 was addressed, confirming slightly higher tumorigenic potential of basal-like cells. Lastly, we combined soft agar colony formation assay with single cell culture to observe individual spheroid growth.

6.2. Zusammenfassung

Lentivirale Vektoren werden häufig als Gentransfervektoren eingesetzt, da sie eine hohe Transduktionseffizienz und Langzeitexpressionsstabilität aufweisen. Sie sind in der Lage, sowohl teilende als auch nicht teilende Zellen zu transduzieren. Da die Insertion in das Genom der Zielzellen nicht vollständig randomisiert erfolgt und auch die Anzahl der Geninsertionen variieren kann, sind lentiviral transferierte Transgene unterschiedlichen epigenetischen Effekten ausgesetzt, die in weiterer Folge zu großer Variation in Bezug auf die Expression oder zu Gen-Silencing führen können. In dieser Arbeit habe ich mich mit der Charakterisierung der Stabilität der Langzeitexpression des lentiviral-übertragenen Reportergens eGFPLuc (eine Fusion aus den fluoreszierenden Protein eGFP und der Firefly-Luciferase Luc), exprimiert unter der Kontrolle des konstitutiv aktiven PGK Poromoters (PGK-eGFPLuc) oder des *wnt*-Signalweg abhängigen CTP Promoters (CTP4-eGFPLuc) in der Brustkrebs-Zelllinie MDA-MB-231 beschäftigt. Während die Expression von PGK-eGFPLuc über die Zeit stabil war, konnte bei CTP4-eGFPLuc keine endgültige Schlussfolgerung zur Langzeitexpressionsstabilität des Transgens gezogen werden. Es konnte auch gezeigt werden, dass in der MDA-MB-231 Zelllinie die Promotoraktivität von PGK circa 15-fach stärkerer als die von CTP4 war. Es wurden auch homogene MDA-MB-231 Reporter-Sublinien aus Einzelzellkulturen etabliert und deren Transgenexpressionsmuster charakterisiert. Dabei zeigte sich (unerwarteterweise), dass ein stark heterogenen Transgen-Expressionsprofil beibehalten wurde.

Im zweiten Teil dieser Arbeit wurden Charakteristika wie Tumorigenität (Koloniebildung) und das Potential zur Metastasenbildung (Zellmotilität) der lentiviral-transduzierten Sublinien mit dem MDA-MB-231 Wildtyp in vitro verglichen. Dazu wurde die Koloniebildung ohne Oberflächenadheränz in Soft Agar und Methyl Cellulose gemessen. Die Zellmotilität wurde mittels Scratch-Wound Assay mit zwei unterschiedlichen Serum-Starvationsansätzen überprüft. Das tumorigene Potential der lentiviral-transduzierten Subtypen war im Vergleich zum Wildtyp signifikant reduziert, das metastasenbildende Potential blieb jedoch unverändert. Ebenso wurden Koloniebildung und Zellmotilität der als luminal klassifizierten Zelllinie MCF7 mit der basalähnlich klassifizierter Zelllinie MDA-MB-231 verglichen. Dabei konnte in MDA-MB-231 Zellen wie erwartet ein geringfügig größeres tumorerzeugendes Potential im Vergleich zu MCF7 beobachtet werden. Schlussendlich wurde der Soft Agar Colony Formation Assay mit Einzellzellkultur kombiniert, um das Wachstum von Spheroiden aus einer einzelnen Zelle beobachten zu können.

7. References

Anders, Carey K., and Lisa A. Carey
2009 Biology, Metastatic Patterns, and Treatment of Patients with Triple-Negative Breast Cancer. Clinical Breast Cancer 9(Suppl 2): S73–S81.

Berry, Charles, Sridhar Hannenhalli, Jeremy Leipzig, and Frederic D. Bushman
2006 Selection of Target Sites for Mobile DNA Integration in the Human Genome. PLoS Computational Biology 2(11): e157.

Bian, Qian, and Andrew S. Belmont
2010 BAC TG-EMBED: One-Step Method for High-Level, Copy-Number-Dependent, Position-Independent Transgene Expression. Nucleic Acids Research 38(11): e127.

Bilandzic, Maree, and Kaye L. Stenvers
2014 Assessment of Ovarian Cancer Spheroid Attachment and Invasion of Mesothelial Cells in Real Time. Journal of Visualized Experiments : JoVE(87). http://www.ncbi.nlm.nih.gov/pmc/articles/PMC4199467/, accessed April 18, 2017.

BioTechniques - TScratch: A Novel and Simple Software Tool for Automated Analysis of Monolayer Wound Healing Assays
N.d. http://www.biotechniques.com/BiotechniquesJournal/2009/April/TScratch-a-novel-and-simple-software-tool-for-automated-analysis-of-monolayer-wound-healing-assays/biotechniques-133324.html?pageNum=4, accessed April 8, 2017.

Borowicz, Stanley, Michelle Van Scoyk, Sreedevi Avasarala, et al.
2014 The Soft Agar Colony Formation Assay. Journal of Visualized Experiments : JoVE(92). http://www.ncbi.nlm.nih.gov/pmc/articles/PMC4353381/, accessed April 3, 2017.

Charrier, S, M Ferrand, M Zerbato, et al.
2011 Quantification of Lentiviral Vector Copy Numbers in Individual Hematopoietic Colony-Forming Cells Shows Vector Dose-Dependent Effects on the Frequency and Level of Transduction. Gene Therapy 18(5): 479–487.

Chavez, Kathryn J., Sireesha V. Garimella, and Stanley Lipkowitz

2010 Triple Negative Breast Cancer Cell Lines: One Tool in the Search for Better Treatment of Triple Negative Breast Cancer. Breast Disease 32(1–2): 35–48.

Cheang, M., S. K. Chia, D. Tu, et al.
2009 Anthracyclines in Basal Breast Cancer: The NCIC-CTG Trial MA5 Comparing Adjuvant CMF to CEF. Journal of Clinical Oncology 27:15s(suppl; abstr 519). http://meetinglibrary.asco.org/content/35150-65, accessed April 5, 2017.

Chira, Sergiu, Carlo S. Jackson, Iulian Oprea, et al.
2015 Progresses towards Safe and Efficient Gene Therapy Vectors. Oncotarget 6(31): 30675–30703.

Chung, Gina G., Maciej P. Zerkowski, Idris Tolgay Ocal, et al.
2004 β-Catenin and p53 Analyses of a Breast Carcinoma Tissue Microarray. Cancer 100(10): 2084–2092.

Clevers, Hans
2006 Wnt/β-Catenin Signaling in Development and Disease. Cell 127(3): 469–480.

Codeluppi, Simone, Ebba Norsted Gregory, Jacob Kjell, et al.
2011 Influence of Rat Substrain and Growth Conditions on the Characteristics of Primary Cultures of Adult Rat Spinal Cord Astrocytes. Journal of Neuroscience Methods 197(1): 118–127.

Counsell, John R., Zeinab Asgarian, Jinhong Meng, et al.
2017 Lentiviral Vectors Can Be Used for Full-Length Dystrophin Gene Therapy. Scientific Reports 7. http://www.ncbi.nlm.nih.gov/pmc/articles/PMC5356018/, accessed April 11, 2017.

Dale, T., K. Patel, B. O'Clair, et al.
2014 323: Simplifying High Throughput 3D Tumour Spheroid Growth and Shrinkage Assays Using Live Content Imaging. European Journal of Cancer 50: S77.

Dawson, S. J., E. Provenzano, and C. Caldas
2009 Triple Negative Breast Cancers: Clinical and Prognostic Implications. European Journal of Cancer 45, Supplement 1. Joint ECCO 15 – 34th ESMO Multidisciplinary Congress Education Book: 27–40.

Dey, Nandini, Benjamin G. Barwick, Carlos S. Moreno, et al.
2013 Wnt Signaling in Triple Negative Breast Cancer Is Associated with Metastasis. BMC Cancer 13: 537.

Ellis, James
2005 Silencing and Variegation of Gammaretrovirus and Lentivirus Vectors. Human Gene Therapy 16(11): 1241–1246.

Emery, David W.
2011 The Use of Chromatin Insulators to Improve the Expression and Safety of Integrating Gene Transfer Vectors. Human Gene Therapy 22(6): 761–774.

Emery, David W., Evangelia Yannaki, Julie Tubb, et al.
2002 Development of Virus Vectors for Gene Therapy of β Chain Hemoglobinopathies: Flanking with a Chromatin Insulator Reduces γ-Globin Gene Silencing in Vivo. Blood 100(6): 2012–2019.

Gaedtke, Lars, Jaroslav Pelisek, Kai S. Lipinski, Christopher J. Wrighton, and Ernst Wagner
2007 Transcriptionally Targeted Nonviral Gene Transfer Using a β-Catenin/TCF-Dependent Promoter in a Series of Different Human Low Passage Colon Cancer Cells. Molecular Pharmaceutics 4(1): 129–139.

Gebäck, Tobias, Martin Michael Peter Schulz, Petros Koumoutsakos, and Michael Detmar
2009 TScratch: A Novel and Simple Software Tool for Automated Analysis of Monolayer Wound Healing Assays. BioTechniques 46(4): 265–274.

Gluz, O., C. Liedtke, N. Gottschalk, et al.
2009 Triple-Negative Breast Cancer—current Status and Future Directions. Annals of Oncology 20(12): 1913–1927.

Graham, IanR., and Alistair Chambers
1997 Constitutive Expression Vectors: PGK. *In* Recombinant Gene Expression Protocols. RockyS. Tuan, ed. Pp. 159–169. Methods in Molecular Biology, 62. Humana Press. http://dx.doi.org/10.1385/0-89603-480-1%3A159, accessed April 10, 2017.

Hanahan, Douglas, and Robert A. Weinberg
2000 The Hallmarks of Cancer. Cell 100(1): 57–70.

Hanahan, Douglas, and Robert A. Weinberg
2011 Hallmarks of Cancer: The Next Generation. Cell 144(5): 646–674.

Hislop, James N., Tarin A. Islam, Ioanna Eleftheriadou, et al.
2014 Rabies Virus Envelope Glycoprotein Targets Lentiviral Vectors to the Axonal Retrograde Pathway in Motor Neurons. The Journal of Biological Chemistry 289(23): 16148–16163.

Holliday, Deborah L, and Valerie Speirs
2011 Choosing the Right Cell Line for Breast Cancer Research. Breast Cancer Research : BCR 13(4): 215.

Howe, Louise R., and Anthony M. C. Brown
2004 Wnt Signaling and Breast Cancer. Cancer Biology & Therapy 3(1): 36–41.

Kantor, Boris, Rachel M. Bailey, Keon Wimberly, Sahana N. Kalburgi, and Steven J. Gray
2014 Methods for Gene Transfer to the Central Nervous System. Advances in Genetics 87: 125–197.

Katz, Richard A., Emily Jack-Scott, Anna Narezkina, et al.
2007 High-Frequency Epigenetic Repression and Silencing of Retroviruses Can Be Antagonized by Histone Deacetylase Inhibitors and Transcriptional Activators, but Uniform Reactivation in Cell Clones Is Restricted by Additional Mechanisms. Journal of Virology 81(6): 2592–2604.

Khramtsov, Andrey I., Galina F. Khramtsova, Maria Tretiakova, et al.
2010 Wnt/β-Catenin Pathway Activation Is Enriched in Basal-Like Breast Cancers and Predicts Poor Outcome. The American Journal of Pathology 176(6): 2911–2920.

King, Taj D., and Yonghe Li
2011 Dysregulation of Wnt Signaling in Breast Cancer. http://www.intechopen.com/books/breast-cancer-carcinogenesis-cell-growth-and-signalling-pathways/dysregulation-of-wnt-signaling-in-breast-cancer, accessed April 4, 2017.

Koval, A. V., P. Vlasov, P. Shichkova, et al.
2014 Anti-Leprosy Drug Clofazimine Inhibits Growth of Triple-Negative Breast Cancer Cells via Inhibition of Canonical Wnt Signaling. Biochemical Pharmacology 87(4): 571–578.

Kramer, Nina, Angelika Walzl, Christine Unger, et al.
2013 In Vitro Cell Migration and Invasion Assays. Mutation Research 752(1): 10–24.

Li, Fuqiang, Mingjie Yang, Lai Wang, et al.
2012 Autofluorescence Contributes to False-Positive Intracellular Foxp3 Staining in Macrophages: A Lesson Learned from Flow Cytometry. Journal of Immunological Methods 386(1–2): 101–107.

Li, Tao, Tao Li, Chunfu Zhang, et al.
2015 Umbilical Cord-Derived Mesenchymal Stem Cells Promote Proliferation and Migration in MCF-7 and MDA-MB-231 Breast Cancer Cells through Activation of the ERK Pathway. Oncology Reports 34(3): 1469–1477.

Liang, Chun-Chi, Ann Y. Park, and Jun-Lin Guan
2007 In Vitro Scratch Assay: A Convenient and Inexpensive Method for Analysis of Cell Migration in Vitro. Nature Protocols 2(2): 329–333.

Liao, J., Q. Wei, J. Fan, et al.
2017 Characterization of Retroviral Infectivity and Superinfection Resistance during Retrovirus-Mediated Transduction of Mammalian Cells. Gene Therapy. http://www.nature.com/gt/journal/vaop/naam/abs/gt201724a.html, accessed April 11, 2017.

Lipinski, Kai S., A. Hakim Djeha, Tariq Ismail, et al.
2001 High-Level, β-Catenin/TCF-Dependent Transgene Expression in Secondary Colorectal Cancer Tissue. Molecular Therapy 4(4): 365–371.

Lipinski, Kai S., Hakim A. Djeha, Jonathan Gawn, et al.
2004 Optimization of a Synthetic β-Catenin-Dependent Promoter for Tumor-Specific Cancer Gene Therapy. Molecular Therapy 10(1): 150–161.

MacDonald, Bryan T., Keiko Tamai, and Xi He
2009 Wnt/β-Catenin Signaling: Components, Mechanisms, and Diseases. Developmental Cell 17(1): 9–26.

Mátrai, Janka, Marinee KL Chuah, and Thierry VandenDriessche
2010 Recent Advances in Lentiviral Vector Development and Applications. Molecular Therapy 18(3): 477–490.

Mori, Seiichi, Jeffrey T. Chang, Eran R. Andrechek, et al.
2009 An Anchorage-Independent Cell Growth Signature Identifies Tumors with Metastatic Potential. Oncogene 28(31): 2796–2805.

Norrman, Karin, Yvonne Fischer, Blandine Bonnamy, et al.
2010 Quantitative Comparison of Constitutive Promoters in Human ES Cells. PLoS ONE 5(8). http://www.ncbi.nlm.nih.gov/pmc/articles/PMC2928720/, accessed April 10, 2017.

Osborne, C. Kent, Kimberly Hobbs, and Jeffrey M. Trent
1987 Biological Differences among MCF-7 Human Breast Cancer Cell Lines from Different Laboratories. Breast Cancer Research and Treatment 9(2): 111–121.

Ovcaricek, Tanja, Snjezana Grazio Frkovic, Erika Matos, Barbara Mozina, and Simona Borstnar
2010 Triple Negative Breast Cancer – Prognostic Factors and Survival. Radiology and Oncology 45(1): 46–52.

Pan, Hong, Wenbin Zhou, Wei He, et al.
2012 Genistein Inhibits MDA-MB-231 Triple-Negative Breast Cancer Cell Growth by Inhibiting NF-κB Activity via the Notch-1 Pathway. International Journal of Molecular Medicine 30(2): 337–343.

Pannell, Dylan, Cameron S. Osborne, Shuyuan Yao, et al.
2000 Retrovirus Vector Silencing Is de Novo Methylase Independent and Marked by a Repressive Histone Code. The EMBO Journal 19(21): 5884–5894.

Pirkmajer, Sergej, and Alexander V. Chibalin
2011 Serum Starvation: Caveat Emptor. American Journal of Physiology - Cell Physiology 301(2): C272–C279.

Pontarin, Giovanna, Paola Ferraro, Chiara Rampazzo, et al.
2011 Deoxyribonucleotide Metabolism in Cycling and Resting Human Fibroblasts with a Missense Mutation in p53R2, a Subunit of Ribonucleotide Reductase. Journal of Biological Chemistry 286(13): 11132–11140.

Qin, Jane Yuxia, Li Zhang, Kayla L. Clift, et al.
2010 Systematic Comparison of Constitutive Promoters and the Doxycycline-Inducible Promoter. PLOS ONE 5(5): e10611.

Ramezani, Ali, Teresa S. Hawley, and Robert G. Hawley
2000 Lentiviral Vectors for Enhanced Gene Expression in Human Hematopoietic Cells. Molecular Therapy 2(5): 458–469.

Rouzier, Roman, Charles M. Perou, W. Fraser Symmans, et al.
2005 Breast Cancer Molecular Subtypes Respond Differently to Preoperative Chemotherapy. Clinical Cancer Research 11(16): 5678–5685.

Siegel, Rebecca L., Kimberly D. Miller, and Ahmedin Jemal
2017 Cancer Statistics, 2017. CA: A Cancer Journal for Clinicians 67(1): 7–30.

Sumiyoshi, Teiko, Nathalia G. Holt, Roger P. Hollis, et al.
2009 Stable Transgene Expression in Primitive Human CD34+ Hematopoietic Stem/Progenitor Cells, Using the Sleeping Beauty Transposon System. Human Gene Therapy 20(12): 1607–1626.

Talmadge, James E, and Isaiah J Fidler
2010 AACR Centennial Series: The Biology of Cancer Metastasis: Historical Perspective. Cancer Research 70(14): 5649–5669.

Yamaguchi, Hideki, and John Condeelis
2007 Regulation of the Actin Cytoskeleton in Cancer Cell Migration and Invasion. Biochimica et Biophysica Acta 1773(5): 642–652.

Yao, Shuyuan, Tanya Sukonnik, Tara Kean, et al.
2004 Retrovirus Silencing, Variegation, Extinction, and Memory Are Controlled by a Dynamic Interplay of Multiple Epigenetic Modifications. Molecular Therapy: The Journal of the American Society of Gene Therapy 10(1): 27–36.

ZHAO, FENG, SHENGLI PAN, YAN GU, et al.
2015 Reactivation of HIC-1 Gene by saRNA Inhibits Clonogenicity and Invasiveness in Breast Cancer Cells. Oncology Letters 9(1): 159–164.

Zufferey, Romain, Thomas Dull, Ronald J. Mandel, et al.
1998 Self-Inactivating Lentivirus Vector for Safe and Efficient In Vivo Gene Delivery. Journal of Virology 72(12): 9873–9880.